

Analytic calculations of the spectra of ultra-high energy cosmic ray nuclei. I. The case of CMB radiation.

R. Aloisio¹, V. Berezhinsky¹ and S. Grigorieva²

¹*INFN, Laboratori Nazionali del Gran Sasso, I-67010 Assergi (AQ), Italy*

²*Institute for Nuclear Research, 60th October Revolution Prospect 7A, 117312 Moscow, Russia*

November 23, 2021

Abstract

We present a new method for the analytic calculation of diffuse spectra of ultra-high energy nuclei. Nuclei propagating in the intergalactic space are photo-disintegrated and decrease their Lorentz factor due to the interaction with Cosmic Microwave Background (CMB) and infrared (IR) radiations. Our method allows the calculation of the diffuse spectra of primary nuclei as well as of secondary nuclei and secondary protons. Our computation scheme is based on four main elements: *(i)* use of the Lorentz factor instead of the energy, *(ii)* calculation of the evolution trajectories in the backward time, that describe how atomic mass number A and the Lorentz factor Γ change with redshift z , *(iii)* use of the kinetic equations for calculation of energy spectra, *(iv)* use of the particles number conservation along each evolution trajectory. In the present paper we consider the interaction of nuclei only with CMB, this case is particularly suitable to explain our computation scheme. In a forthcoming paper (II) infrared radiation will be also included. The main physical results obtained in this paper are as follows. The Helium nuclei strongly dominate in the flux of secondary nuclei at energies $1 \times 10^{18} - 3 \times 10^{19}$ eV. All the other secondary nuclei have a sharp peak in the $E^3 J(E)$ spectrum at $\Gamma \sim 4 \times 10^9$, which coincides with a characteristic scale of nuclei propagation: the critical Lorentz factor. The spectrum of secondary protons at high energy has a universal form, i.e. it does not depend on the primary nuclei species A_0 accelerated at the source.

1 Introduction

The terrestrial observation of particles with ultra high energies ($E > 10^{18}$ eV) has a fundamental importance in high energy astrophysics and, maybe, more generally in physics. These particles, hereafter referred to as Ultra High Energy Cosmic Rays (UHECR), attract much attention in the recent years as the most energetic particles ever observed and because they are messengers from cosmic accelerators to the highest energies, that could be at the same time also powerful astrophysical sources in different frequency ranges.

The observational data on UHECR can be divided into three categories: spectra, chemical composition and correlation with astrophysical sources.

Several theoretically well established features are predicted for the energy spectra of UHE *protons* interacting with the Cosmic Microwave Background (CMB) radiation, most noticeably they are: (i) the Greisen-Zatsepin-Kuzmin (GZK) feature [1], a sharp steepening of the spectrum at $E \simeq 5 \times 10^{19}$ eV due to the photo-pion production process [1]; (ii) a rather faint feature, the dip, at energies $1 \times 10^{18} - 4 \times 10^{19}$ eV, caused by the e^+e^- pair production process [2], and (iii) an even more faint and sharp peak at energy 6.3×10^{19} eV produced by an interference effect in the proton interaction with CMB [3].

Two of these features, the GZK cutoff and the dip, most probably are already detected. The observation of the GZK feature in the differential spectrum of HiRes [4] is strengthened by the measured value of $E_{1/2}$ in the integral spectrum, which precisely coincides with the theoretical prediction. The Auger data [5, 6, 7] also show a steepening of the spectrum, which does not contradict the theoretically predicted position of GZK feature.

The dip is well confirmed by the data of Hires, AGASA and Yakutsk detectors [8, 9, 10], but shows a large χ^2 in the comparison with the Auger data [11].

One may notice that both features discussed above are signatures of a pure proton composition. Therefore, agreement with the data can be considered as an indirect evidence for this composition.

The direct observation of UHECR chemical composition is a very difficult task. At present, observations are rather contradictory. While HiRes [12], HiRes-MIA [13] and Yakutsk [14] detectors favor a proton-dominated flux at energies $E > 10^{18}$ eV, Fly's Eye [15], Haverah Park [16] and AGASA [17] and, recently, Auger [18] indicate a mixed composition (for a review see [19] and [20]).

From a theoretical point of view, there are two models with different predictions for the mass composition. The dip model predicts (almost) pure proton composition starting from energies $E \geq 10^{18}$ eV [21]; the second model [22] predicts a mixed composition with a dominance of the proton component only at the highest energies. As shown in [7], both models contradict the Auger data on mass composition, however assuming a systematic error in the measured x_{\max} larger than the present estimation ($\Delta x_{\text{syst}} \approx 11$ g/cm² [18]) the two models, dip and mixed composition, cannot be excluded. The mixed model has an advantage in explanation of the observed mass composition due to presence of many free parameters. They can be adjusted to explain any reasonable mass composition.

Independently of the theoretical interpretation, Auger data on mass composition show some contradiction with other data obtained by the same observatory. On one hand, x_{\max} measured at the highest energy $E = 4 \times 10^{19}$ eV shows heavier composition than at lower energies, approaching a pure Iron composition [18]. On the other hand, the observation of the GZK cutoff as well as the correlation with AGN [23] seem both to be a confirmation that starting from energy $(5 - 6) \times 10^{19}$ eV the composition is strongly dominated by protons.

The discussion above demonstrates the importance of a theoretical study of nuclei as carriers of the UHE signal. The theoretical interest to UHE nuclei is also supported by the difficulties in reaching ultra high energies by the acceleration of protons in astrophysical models. In the case of nuclei this problem is softened because the maximum acceleration energy increases by a factor Z , the charge number of the accelerated nucleus, which is 26 in the case of Iron.

Historically, the interest in UHE nuclei started from the hope to solve the UHECR puzzle, i.e. the absence of the GZK cutoff in observations, with the help of nuclei as signal carrier. In this case the energy of a CMB photon in the rest system of a nucleus with atomic mass number A is A times lower than for a proton of the same energy, thus

photo-pion production is suppressed.

The first calculations of the UHE nuclei photo-disintegration by the CMB radiation has been performed by Stecker [24] and by Puget and Stecker [25], where infrared radiation was also included. The first calculations of diffuse nuclei spectrum have been made by Berezhinsky, Grigorieva, Zatsepin [26] and Hillas [27], both works have been presented at the same conference and published in the same volume of the proceedings. It was demonstrated that the steepening in the heavy-nuclei spectra such as Fe, Al, C etc occurs at energies lower than the GZK cutoff for protons.

Propagating in intergalactic space, UHE nuclei interact with the CMB and IR radiations experiencing two main processes: (i) photo-disintegration and (ii) e^+e^- pair production, that reduce the nucleus kinetic energy. The systematic study of the photo-disintegration started from the pioneering works by Stecker [24, 25, 28, 29]. These works are based on a very convenient parameterization of the photo-nuclear cross-sections, widely used in the study of UHE nuclei propagation. Recently, the refined parameterization of this cross-section was presented in [30].

Using the parameterization of the photo-nuclear cross section by Stecker [28], updated in 1999 [29], or using other approximations as in [30], many papers have been published in the last decade, all (except [31, 32]) based on a Monte Carlo (MC) approach to the study of UHE nuclei propagation in astrophysical backgrounds [33, 34, 29, 35, 36, 37, 38, 30, 39, 40, 22, 41, 42, 43, 44].

We present here a new method for the analytic calculation of UHE nuclei spectra. It is based on the kinetic equation, which gives the nuclei energy spectra, and on the computation of the evolution trajectories of nuclei. The evolution trajectories describe how the Lorentz factor (Γ) and atomic mass number (A) are changing during propagation. We will present our new analytic calculations in the form of two papers. In this paper (paper I) we include only CMB as the radiation with which UHE nuclei interact. The main emphasis of this paper is given to the theoretical issues of our method. It is more convenient to do it with CMB only, because the Planck spectrum and the exact knowledge of the cosmological evolution of this radiation make formulae simpler and the description of the method more transparent. The phenomenological predictions obtained with CMB only are always relevant for the highest energy part of the spectra.

In a forthcoming paper (paper II) we will include the interaction with both CMB and IR radiations, and focus more on the observational applications of our new computation scheme.

The paper is organized as follows: in section 2 we calculate the energy losses of nuclei on the CMB radiation, and compute the evolution trajectories. In section 3 we calculate the flux of secondary nuclei. This is a benchmark section where our computation method is clearly described. In sections 4 and 5, respectively, the spectra of secondary protons and primary nuclei are calculated. Conclusions with a discussion of our main results are presented in section 6. In the appendixes we give a detailed calculation and discussion of the following technical problems: in appendix A - the ratio of energy intervals at different redshifts and in appendix B - the solutions of kinetic equations.

2 Energy losses and evolution trajectories

Propagating through background radiations, mainly CMB and IR, nuclei decrease their Lorentz factor Γ , due to e^+e^- pair production, and atomic number A , due to photo-disintegration. Lorentz factor decreases also due to the expansion of the universe (adia-

batic energy losses). In this section we study the energy losses and the evolution of nuclei due to their propagation, considering the evolution trajectories in time (or redshift z) along which A and Γ are changing. We will consider these trajectories in the backward time, starting from the point of observation $(\Gamma, A, z = 0)$ and increasing z , so that Γ and A increase too.

An important ingredient of our method consists in the use of the Lorentz factor of the particles instead of their energy. This approach gives many simplifications in the theoretical study, in particular the approximate equality of Lorentz factors of all three particles participating in photo-disintegration process $A \rightarrow (A - 1) + N$.

2.1 Energy losses on CMB

In this paper we consider interaction of nuclei only with CMB. Adiabatic energy losses and pair production change only Lorentz factor and photo-disintegration changes only atomic number A . Then for $E = \Gamma A m_N$ we have

$$\frac{1}{E} \frac{dE}{dt} = \frac{1}{\Gamma} \frac{d\Gamma}{dt} + \frac{1}{A} \frac{dA}{dt}. \quad (1)$$

For energy losses of nuclei or protons interacting with CMB one has at $z = 0$ in units $\hbar = c = k = 1$ [45]:

$$\beta_0(\Gamma) = -\frac{1}{E} \frac{dE}{dt} = \frac{T}{2\pi^2 \Gamma^2} \int_{\epsilon_0}^{\infty} d\epsilon \sigma(\epsilon) f(\epsilon) \epsilon \left[-\ln \left(1 - \exp\left[-\frac{\epsilon}{2\Gamma T}\right] \right) \right], \quad (2)$$

where ϵ is the photon energy in the nucleus or proton rest frame, ϵ_0 is the threshold of the considered reaction, $f(\epsilon)$ is the mean fraction of energy in the laboratory system lost by a nucleus in a single interaction, i.e. inelasticity, $\sigma(\epsilon)$ is the cross-section and $T = 2.726^\circ\text{K}$ is the CMB temperature.

At redshift z the number of CMB photons is $(1+z)^3$ larger than at $z = 0$ and the energies of these photons are $(1+z)$ times higher. Then the energy loss at arbitrary z is given by

$$\beta(\Gamma, z) = (1+z)^3 \beta_0[(1+z)\Gamma] \quad (3)$$

We specify now the three processes relevant for our calculations: expansion of the universe (adiabatic energy losses), pair production and photo-disintegration.

(i) *Adiabatic energy losses.*

Adiabatic energy losses are given by

$$\beta_{\text{ad}}(z) = -\frac{1}{\Gamma} \frac{d\Gamma}{dt} = H(z), \quad (4)$$

where $H(z) = H_0 \sqrt{(1+z)^3 \Omega_m + \Omega_\Lambda}$ is the Hubble parameter at redshift z with $H_0 = 72$ km/sMpc, $\Omega_m = 0.238$ and $\Omega_\Lambda = 0.716$ according to WMAP data [46].

(ii) *Electron-positron pair production*

This process can occur if the energy of the background photon is larger than 1 MeV in the rest system of the UHE particle. The inelasticity and cross-section for a nucleus are simply related to the corresponding quantities for the proton pair-production:

$$f_{\text{pair}}^A(\epsilon) = \frac{1}{A} f_{\text{pair}}^p(\epsilon), \quad \sigma_{\text{pair}}^A(\epsilon) = Z^2 \sigma_{\text{pair}}^p(\epsilon), \quad \beta_{\text{pair}}^A(\Gamma) = \frac{Z^2}{A} \beta_{\text{pair}}^p(\Gamma), \quad (5)$$

where Z is a charge number of the nucleus, m_N is the nucleon mass, σ_{pair}^i is the pair production cross section for protons ($i = p$) or nuclei ($i = A$). Using these equations we can rewrite Eq. (2) as

$$\beta_{\text{pair}}^A(\Gamma) = -\frac{1}{\Gamma} \frac{d\Gamma}{dt} = \frac{Z^2}{A} \frac{T}{2\pi^2\Gamma^2} \int_{\epsilon_0}^{\infty} d\epsilon \sigma_{\text{pair}}^p(\epsilon) f_{\text{pair}}^p(\epsilon) \epsilon \left[-\ln \left(1 - \exp\left[-\frac{\epsilon}{2\Gamma T}\right] \right) \right]. \quad (6)$$

The expression above is valid for $z = 0$. For arbitrary z one should use Eq. (3). In our calculations we use the function $\beta_{\text{pair}}^p(\Gamma)$ for protons as computed in [9].

(ii) *Photo-disintegration.*

The photo-disintegration energy losses on CMB at $z = 0$ are given by

$$\beta_{\text{dis}}^A(\Gamma) = -\frac{1}{A} \frac{dA}{dt} = \frac{T}{2\pi^2\Gamma^2} \frac{1}{A} \int_{\epsilon_0(A)}^{\infty} d\epsilon \sigma_{\text{dis}}(\epsilon, A) \nu(\epsilon) \epsilon \left[-\ln \left(1 - \exp\left[-\frac{\epsilon}{2\Gamma T}\right] \right) \right], \quad (7)$$

where $\nu(\epsilon)$ is the average multiplicity of the emitted nucleons.

At arbitrary z the pair-production energy losses $\beta_{\text{pair}}(\Gamma, z)$ and photo-disintegration energy losses $\beta_{\text{dis}}^A(\Gamma, z)$ are given by Eq. (3).

The quantity β_{dis}^A determines the time of total photo-disintegration of a nucleus $\tau_{\text{tot}} = 1/\beta_{\text{dis}}^A$, while $\tau_A = 1/(A\beta_{\text{dis}}^A) = (dA/dt)^{-1}$ gives the mean time for losing one nucleon.

In the present paper we use the remarkable collection of data on nuclear cross-section and their parametrization from the works by Stecker et al [28, 29].

Depending on the photon energy ϵ in the nucleus rest frame, one can distinguish two different regimes of photo-disintegration, namely the low-energy regime $\epsilon < 30$ MeV and the high-energy regime: $30 < \epsilon < 150$ MeV. At energies $\epsilon > 150$ MeV the photo-disintegration process is not important [28, 29].

In the low-energy regime the leading processes of photo-disintegration are represented by one and two nucleon emission, $A + \gamma \rightarrow (A - 1) + N$, $A + \gamma \rightarrow (A - 2) + 2N$, and the photo-disintegration cross-section is dominated by the Giant Dipole Resonance (GDR) [28, 29]. At higher energies a multi-nucleon emission regime takes place (see [28, 29]). In this regime the photo-disintegration cross-section can be approximated as constant [28, 29]. The main contribution to photo-disintegration is given by the GDR cross-section with mean number of emitted nucleons $2 > \nu > 1$.

We have calculated the energy losses for all nuclei with existing data, presenting some of them in Figs. 1 and 2 as function of the Lorentz factor.

As we will discuss below, an important quantity that characterizes nuclei propagation is the *critical Lorentz factor* Γ_c defined as the Lorentz factor where photo-disintegration energy losses become equal to the sum of adiabatic and pair-production energy losses:

$$\beta_{\text{dis}}(\Gamma_c) = \beta_{\text{ad}} + \beta_{\text{pair}}(\Gamma_c) \quad (8)$$

Nucleus	D	${}^3\text{He}$	${}^4\text{He}$	${}^9\text{Be}$	${}^{14}\text{C}$	${}^{24}\text{Mg}$	${}^{40}\text{Ca}$	${}^{56}\text{Fe}$
Γ_c	4.5×10^8	1.4×10^9	4.8×10^9	5.1×10^8	3.4×10^9	3×10^9	4×10^9	3×10^9

Table 1: Values of Γ_c for some selected nuclei

The values of Γ_c calculated for some nuclei are listed in Table 1. From this Table and Fig. 2 one may notice that Γ_c is almost the same for all heavy nuclei with a value around $(3 - 4) \times 10^9$. For Γ_c at epoch z we use the notation $\Gamma_c(z)$.

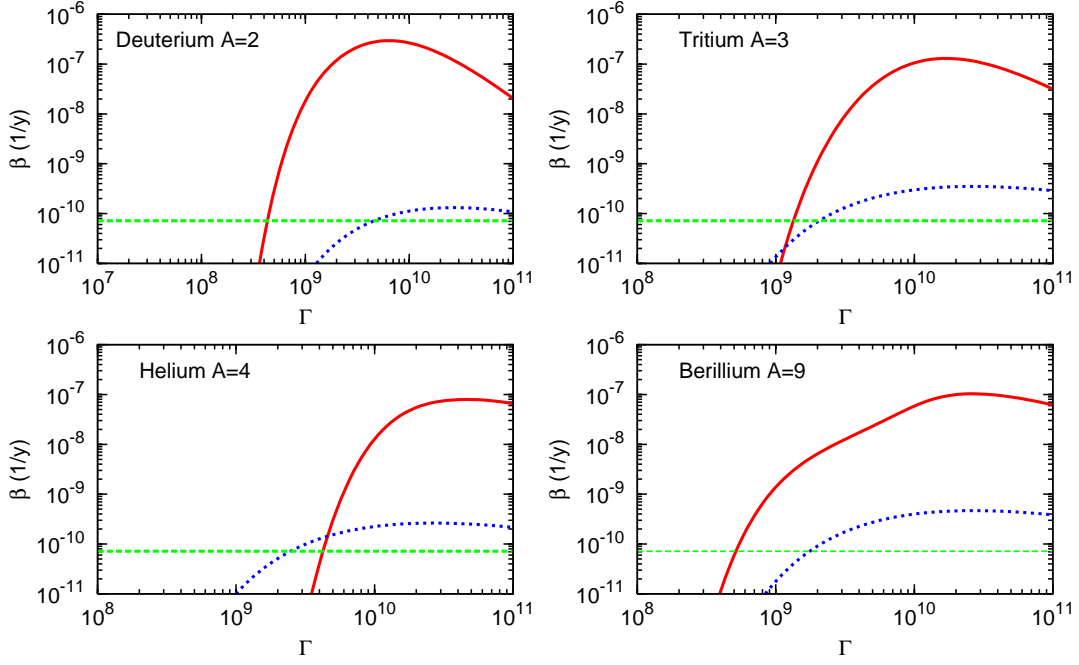


Figure 1: Energy losses for light nuclei due to photo-disintegration and pair production on CMB (red full line and blue dotted line, respectively) and adiabatic energy losses given by H_0 (green dashed line).

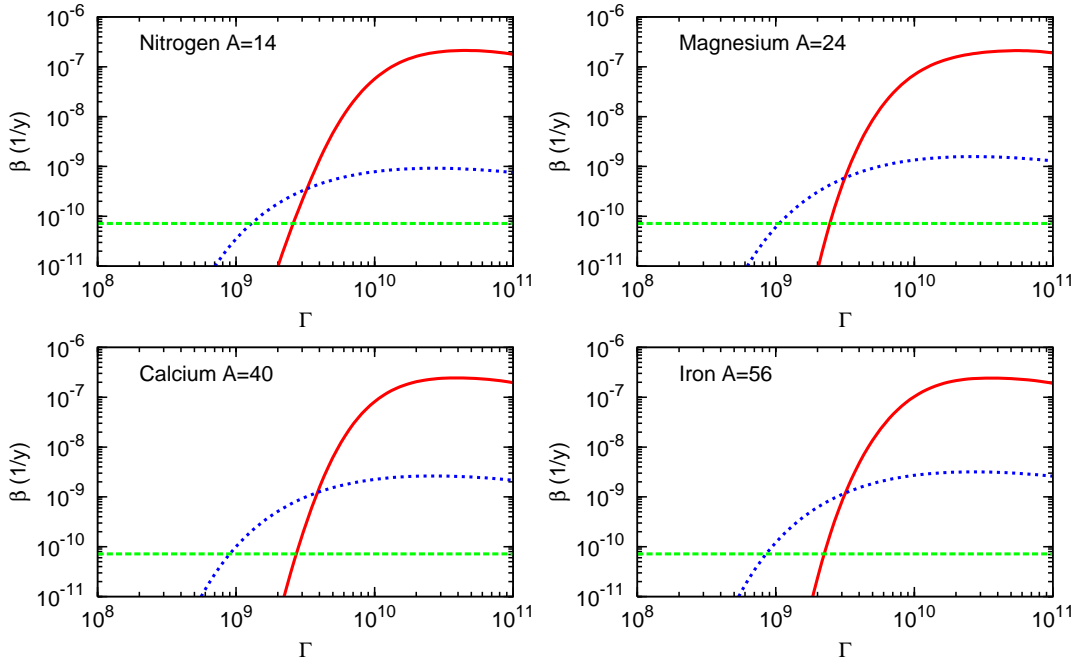


Figure 2: The same as in Fig. 1 for heavy nuclei.

2.2 Evolution trajectories

A primary nucleus A_0 accelerated to large Lorentz factor Γ_g at redshift z_g is soon photo-disintegrated and then evolves as secondary nucleus with decreasing A and Γ as redshift z decreases.

Our study of evolution goes in the backward time, whose role is played by redshift. We consider as initial state a secondary nucleus A with Lorentz factor Γ and evolve it to larger z with increasing of $A(z)$ and $\Gamma(z)$ until $A(z)$ reaches A_0 at z_g (index g here and henceforth implies *generation*, i.e. acceleration, of A_0). Evolution of Γ from $z = 0$ to z_g gives Γ_g of nucleus A_0 . This backward-time evolution is governed by two coupled differential equations, which for a variable z reads

$$\frac{1}{A} \frac{dA}{dz} = \left| \frac{dt}{dz} \right| \beta_{\text{dis}}(\Gamma, A, z) \quad , \quad \frac{1}{\Gamma} \frac{d\Gamma}{dz} = \left| \frac{dt}{dz} \right| \beta_{\text{pair}}(\Gamma, A, z) + \frac{1}{1+z}, \quad (9)$$

with relation between time and redshift dt/dz given by

$$\frac{dt}{dz} = - \frac{1}{H_0(1+z)\sqrt{(1+z)^3\Omega_m + \Omega_\Lambda}}. \quad (10)$$

The last term in rhs of the second equation in (9) corresponds to adiabatic energy losses $d\Gamma/dt = -\Gamma H(z)$.

The differential equations (9) give in principle the solutions $A(z)$ continuous in A . In our work $A(z)$ trajectories plays auxiliary role, determining values of z_A , where $A(z)$ reaches different integer values of A .

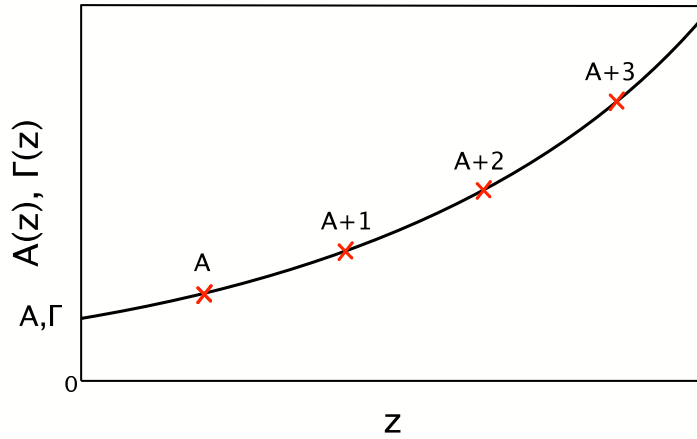


Figure 3: A sketch of $\Gamma(z)$ and $A(z)$ evolution with $\Gamma(z)$ evolution shown by continuous curve and integer values of A shown by crosses. $A(z)$ is calculated as continuous quantity, but transition e.g. from $A + 1$ to A nuclei (or $A + 2 \rightarrow A$) is assumed to occur instantaneously and marked by crosses. The nucleus between $A + 1$ (or $A + 2$) and A decays is considered as nucleus with fixed A .

The numerical solution of the coupled equations (9) with initial values A and Γ at z_0 gives the evolution trajectories $A(z) = \mathcal{A}(A, \Gamma, z_0, z)$ and $\Gamma(z) = \mathcal{G}(A, \Gamma, z_0, z)$, where the first three arguments describe the initial condition, in most cases with $z_0 = 0$. A trajectory is sketched in Fig. 3 as a continuous quantity $\mathcal{G}(\Gamma, A, z)$ with integer A marked

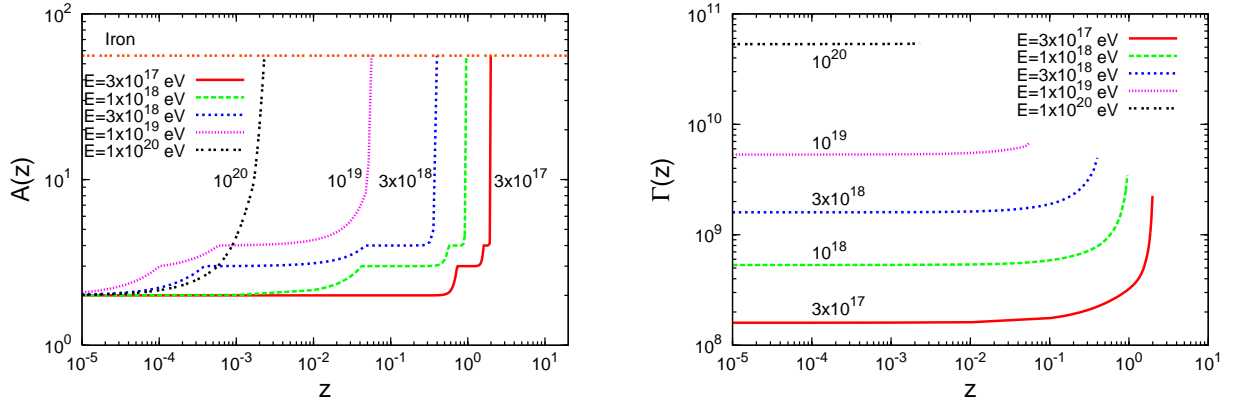


Figure 4: Calculated evolution of the atomic mass number $A(z)$ (left panel) and Lorentz factor $\Gamma(z)$ (right panel) for a deuterium nucleus observed at $z = 0$ with various energies as labeled.

by crosses. In the kinetic equation approach we will interpret this trajectory assuming that nucleus A is produced in instantaneous decay of nucleus $A + 1$, then it lives as A and finally instantaneously decays to $A - 1$. The intervals between crosses are determined by continuous changing of A with resultant $\Delta A = 1$ (or $\Delta A = 2$). This is most natural interpretation, because a nucleus with continuously changing A just does not exist in nature, while instantaneous production of nucleus A from decay of $A + 1$ is a realistic assumption, as well as an assumption that after decay of $A + 1$ in the forward running time a nucleus A propagates with fixed A until instantaneous $A \rightarrow (A - 1)$ decay (we always imply below the case of $A + 2$, too).

How in this picture one should treat the photo-disintegration rate given by β_{dis}^A ? For calculation of $\mathcal{A}(A, \Gamma, z_0, z)$ trajectory we need β_{dis}^A for continuous values of A , while β_{dis}^A is known only for a set of discrete values of A . We use two methods of interpolation of β_{dis}^A between the discrete values of A .

In the first method we use our basic interpretation of $A(z)$ trajectory, namely that $A(z)$ between the photo-disintegrations of A and $A + 1$ we consider as a nucleus with the fixed value of A . We assume accordingly that β_{dis}^A is a quantity with a fixed A at $A < A(z) < A + 1$, which changes by jump at $A + 1$. We refer to this approximation as “jump-changed β ”.

In the second method we use a more smooth interpolation between values of β_{dis}^A at A and $A + 1$. Both methods give similar results (almost identical for calculations of z_g and Γ_g), and in practical calculations we used the first method, as more physical.

In Fig. 4 the calculated evolution trajectories $\mathcal{A}(A, \Gamma, z_0, z)$ and $\mathcal{G}(A, \Gamma, z_0, z)$ are shown for the initial condition $A = 2$ (Deuterium), $z_0 = 0$ and different values of Γ , corresponding to energy E indicated in the figure. $A(z)$ is evolved to $A_0 = 56$ (Iron) and z_g is determined. Then $\Gamma_g = \mathcal{G}(A, \Gamma, z_0, z_g)$ is calculated as shown by the end points in the right panel of Fig. 4.

We describe the obtained results, which are typical for other trajectories, too.

At low initial energy (e.g. $E = 3 \times 10^{17}$ eV), the evolution of A is quite slow, this quantity remains constant in a wide redshift interval and only when the Lorentz factor $\Gamma(z)$ reaches the critical value $\Gamma_c^{A+1}(z)$, the photo-disintegration process becomes dominant with a sharp increase of the atomic mass number. In the $A(z)$ evolution, and particularly in the case of low initial energies, several features are seen in the raising part of the curve.

These features are determined by the way of approximation of β_{dis}^A as a function of A . In particular, in the lowest-energy curves in the left panel of Fig. 4 (obtained for a jump behaviour of β) one observes a jump from $A = 2$ to $A = 3$, which corresponds to abrupt change in β_{dis}^A at integer value $A = 3$. Another jump from $A = 3$ to $A = 4$ also corresponds to a jump in β_{dis}^A .

At highest energy $E = 1 \times 10^{20}$ eV, $\Gamma > \Gamma_c$ and the photo-disintegration process is dominant and very fast. Deuterium is converted into Iron within a very short redshift interval $z \sim 10^{-3}$ and the Lorentz factor remains unchanged (see right panel of Fig. 4). The photo-disintegration in its high-energy regime is characterized by constant cross-section, β_{dis}^A is continuous function of A and transition is smooth.

From the point of view of the final result of our work as calculation of UHE spectra of nuclei, the evolution trajectories are needed for calculation of two parameters, z_g and Γ_g . The former is calculated from $\mathcal{A}(\Gamma, A, z_g) = A_0$ (left panel of Fig. 4). The latter is calculated as $\Gamma_g = \mathcal{G}(\Gamma, A, z_g)$ (the end-points of trajectories in the right panel of Fig. 4). While the shape of trajectories is sensitive to interpolation of β_{dis}^A between discrete A , the values of z_g and Γ_g remain the same for various interpolations, as we tested it by several models of interpolation.

In the calculations of evolution trajectories we always include two additional conditions: maximum energy of acceleration $E_{\text{max}}^{\text{acc}}$ (in terms of $\Gamma_{\text{max}}^{\text{acc}}$) and nucleus stability restriction. The first restriction is imposed as follows. With z_g determined from $\mathcal{A}(A, \Gamma, z_g) = A_0$ we calculate $\Gamma_g = \mathcal{G}(A, \Gamma, z_g)$. If $\Gamma_g \geq \Gamma_{\text{max}}^{\text{acc}}$ this trajectory is forbidden, and the contribution to flux along this trajectory is set to zero. The second compulsory restriction, caused by nucleus stability, is considered in the next subsection.

2.3 Nucleus stability restriction

If in the chain of nucleus evolution from (A, Γ) to (A_0, Γ_g) , with small enough Γ , there is an intermediate nucleus $A' > A$ with anomalously large threshold of photo-disintegration ϵ_0 , the evolution may be blocked and fail. In our computation scheme we check the trajectories by this condition selecting only the allowed ones. In the case (A, Γ) is connected with A_0 by a forbidden trajectory the flux of UHE A -nuclei is set to zero.

If a nucleus has a Lorentz factor $\Gamma < \Gamma_c$, it is stable, i.e. it is not photo-disintegrated during the Hubble time. It is easy to understand it looking at one of the graphs in Fig. 2, for example, the one for ^{40}Ca . In this case Γ_c is approximately given by the point of intersection of the pair-production and photo-disintegration curves at $\Gamma \approx 4 \times 10^9$. Consider now the evolution of the ^{40}Ca nucleus with $\Gamma \sim 1 \times 10^9$ forward in time. From Fig. 2 it is clear that such nucleus is stable: diminishing of the Lorentz factor goes faster than the changing of A and the nucleus slows down, with a further decrease of $\beta_A(\Gamma)$. However, if one considers the evolution of this nucleus backward in time, the picture will be different. The Lorentz factor of this nucleus increases with z as $\Gamma(z) = \mathcal{G}(A, \Gamma, z_0, z)$, while A remains practically unchanged, because $\beta_A \ll \beta_{\text{pair}}$. Simultaneously $\Gamma_c(z)$ decreases with increasing z , because the intersection point of β_A and β_{pair} is shifted to lower energies by a factor $(1+z)$. As a result at some *critical redshift* $z_c(\Gamma)$, determined by the condition $\beta_{\text{dis}}^A(\Gamma, z) = \beta_{\text{ad}}(z) + \beta_{\text{pair}}^A(\Gamma, z)$, the considered nucleus becomes unstable.

In the realistic case of evolution, a secondary nucleus A is produced by the photo-disintegration transition $A + 1 \rightarrow A$, in this case we should compare $\Gamma_A(z)$ with Γ_c^{A+1} , and the equation for the critical redshift z_c becomes

$$\mathcal{G}(A, \Gamma, z_0, z_c) = \Gamma_c^{A+1}(z_c), \quad (11)$$

where $z_0 = 0$. Therefore, to produce the secondary A with Lorentz factor $\Gamma < \Gamma_c$ at $z_0 = 0$ the parent nucleus $A + 1$ must decay at $z \geq z_c$ determined by the Eq. (11).

The trajectory can be blocked not only by $A + 1$ nucleus, but also by $A' > A + 1$, if A' -nucleus has an anomalously high Γ_c . A realistic example is given by the evolution trajectory of Deuterium $D \rightarrow {}^3\text{He} \rightarrow {}^4\text{He}$, where Γ_c for ${}^4\text{He}$ is much larger than for ${}^3\text{He}$ and D (see Table 1). The condition of the allowed trajectory remains as that in Eq. (11) $\mathcal{G}(D, \Gamma, z_0, z) \geq \Gamma_c^{4\text{He}}(z)$, where z is the redshift of ${}^4\text{He} \rightarrow {}^3\text{He} + N$ photo-disintegration.

3 Secondary Nuclei

We start with the calculations of the secondary-nuclei flux as the most general and technically most interesting part of our calculations. We discuss also here the general concept and basic details which will be used in the calculations for secondary protons and primary nuclei. The main assumptions are also given here. This is a benchmark for all other calculations in the paper.

3.1 Concept and assumptions

We consider an expanding universe homogeneously filled by the sources of accelerated primary UHE nuclei A_0 with a generation rate per unit of comoving volume $Q_{A_0}(\Gamma, z)$ given by

$$Q_{A_0}(\Gamma, z) = \frac{(\gamma_g - 2)}{m_N A_0} \mathcal{L}_0 \Gamma^{-\gamma_g}, \quad (12)$$

where $\gamma_g > 2$ is the generation index, m_N is the nucleon mass and \mathcal{L}_0 is the source *emissivity*. i.e. the energy generated per unit of comoving volume and per unit time at $z = 0$. In Eq. (12) $\Gamma_{\min} \sim 1$ is assumed. In all the calculations below we assume also the existence of a maximum energy of acceleration $E_{\max}^{\text{acc}} = Z_0 \times 10^{21}$ eV (or $\Gamma_{\max}^{\text{acc}} = (Z_0/A_0) \times 10^{12}$) with the condition $Q_{A_0}(\Gamma_g) = 0$ at $\Gamma_g \geq \Gamma_{\max}^{\text{acc}}$.

Propagating in the space, a nucleus A_0 experiences evolution, producing the secondary nuclei with different A and we calculate here their flux and energy spectrum. The basic instrument for these calculations is given by kinetic equations, which take into account generation and photo-disintegration of the secondary nuclei.

For calculation of the generation function and limits of integration in the solution of kinetic equation, the evolution-trajectory formalism, developed in section 2.2, is used. The trajectories $A(z) = \mathcal{A}(\Gamma, A, z_0, z)$ and $\Gamma(z) = \mathcal{G}(\Gamma, A, z_0, z)$ allows us to calculate the generation parameters z_g and Γ_g , when $A(z)$ reaches A_0 . We will describe below how the limits of integration are calculated with help of evolution trajectories.

The trajectory $A(z)$ is calculated as continuous quantity, but we interpret it as $A = \text{const}$ between moment of instantaneous production $(A + 1) \rightarrow A + N$ and the moment of instantaneous photo-disintegration $A \rightarrow (A - 1) + N$. Since a recoil momentum in these processes is negligibly small, one has approximate equality of Lorentz-factors of all three particles

$$\Gamma_{A+1} \approx \Gamma_A \approx \Gamma_N. \quad (13)$$

The kinetic equation for the comoving space density of secondary nuclei A , $n_A(\Gamma_A, t)$, reads

$$\frac{\partial n_A(\Gamma_A, t)}{\partial t} - \frac{\partial}{\partial \Gamma_A} [b_A(\Gamma_A, t) n_A(\Gamma_A, t)] + \frac{n_A(\Gamma_A, t)}{\tau_A(\Gamma_A, t)} = Q_A(\Gamma_A, t), \quad (14)$$

where $b_A = (\beta_{\text{pair}} + \beta_{\text{ad}})\Gamma_A$ is the rate of the Lorentz-factor loss (analogue of energy loss), the lifetime of nucleus A is approximately given by

$$\tau_A^{-1}(\Gamma_A, z) = dA/dt = A\beta_{\text{dis}}(A, \Gamma_A, z), \quad (15)$$

and $Q_A(\Gamma_A, t)$ is the generation rate of nuclei A per unit of comoving space. It is given by the decay rate of the parent nuclei $A + 1$ (or $A + 2$):

$$Q_A(\Gamma_A, z)d\Gamma_A dt = Q_{A+1}^{\text{dec}}(\Gamma_{A+1}, z)d\Gamma_{A+1} dt, \quad (16)$$

where $\Gamma_A \approx \Gamma_{A+1}$ as given by Eq. (13).

To determine the injection rate of secondary nuclei Q_A , we can use the conservation of the number of particles along the evolution trajectory, which requires that the number of nuclei decaying during dt at epoch z is equal to the number of nuclei A_0 produced by acceleration during dt_g at the epoch z_g : $dN'_A = dN_{A_0}$. This relation is especially transparent in the case of an *instantaneous* $A + 1 \rightarrow A$ decay.

Using Eq. (16) we obtain

$$Q_A(\Gamma_A, z)d\Gamma_A dt = Q_{A_0}(\Gamma_g, z_g)d\Gamma_g dt_g \quad (17)$$

where (Γ_A, z) and (Γ_g, z_g) are connected by evolution trajectory. From Eq. (17) using the time dilatation relation

$$dt_g/dt = (1+z)/(1+z_g), \quad (18)$$

we obtain the generation rate of nuclei A as:

$$Q_A(\Gamma_A, z) = Q_{A_0}(\Gamma_g, z_g) \frac{1+z}{1+z_g} \frac{d\Gamma_g}{d\Gamma_A} \quad (19)$$

with $d\Gamma_g/d\Gamma_A$ given in appendix A.

3.2 Kinetic equation solution and integration limits

The solution of the kinetic equation (14) is found in appendix B and can be presented as

$$n_A(\Gamma) = \int_{z_{\text{min}}}^{z_{\text{max}}} dz \left| \frac{dt}{dz} \right| Q_A(\Gamma_A, z) \frac{d\Gamma_A}{d\Gamma} e^{-\eta(\Gamma_A, z)} \quad (20)$$

where $n_A(\Gamma)$ is given for $z = 0$, z is the redshift of A -nuclei production, $\Gamma_A = \mathcal{G}(A, \Gamma, z_0, z)$ is the Lorentz factor of the nucleus A obtained by evolving A from $z_0 = 0$ (when Lorentz factor is Γ) to z . The quantity $\eta(\Gamma_A, z)$ takes into account the photo-disintegration lifetime of the nucleus A , and it is given by

$$\eta(\Gamma_A, z) = \int_0^z dz' \left| \frac{dt'}{dz'} \right| \frac{1}{\tau_A(\Gamma_A, z')} = \int_0^z dz' \frac{dA}{dz'} \quad (21)$$

The cases $\eta = 1$ and $\eta = 2$ correspond to one- and two-nucleon emission, respectively.

The generation rate Q_A is given by Eq. (19) with derivative $d\Gamma_A/d\Gamma$ calculated in appendix A.

Formally the limits of integration in Eq. (20) are 0 and ∞ . We use as an effective upper limit z_{A_0} , the largest physically accessible value given by the solution of the equation $\mathcal{A}(A, \Gamma, z_0 = 0, z) = A_0$, when the running $A(z)$ reaches A_0 . Another candidate on the

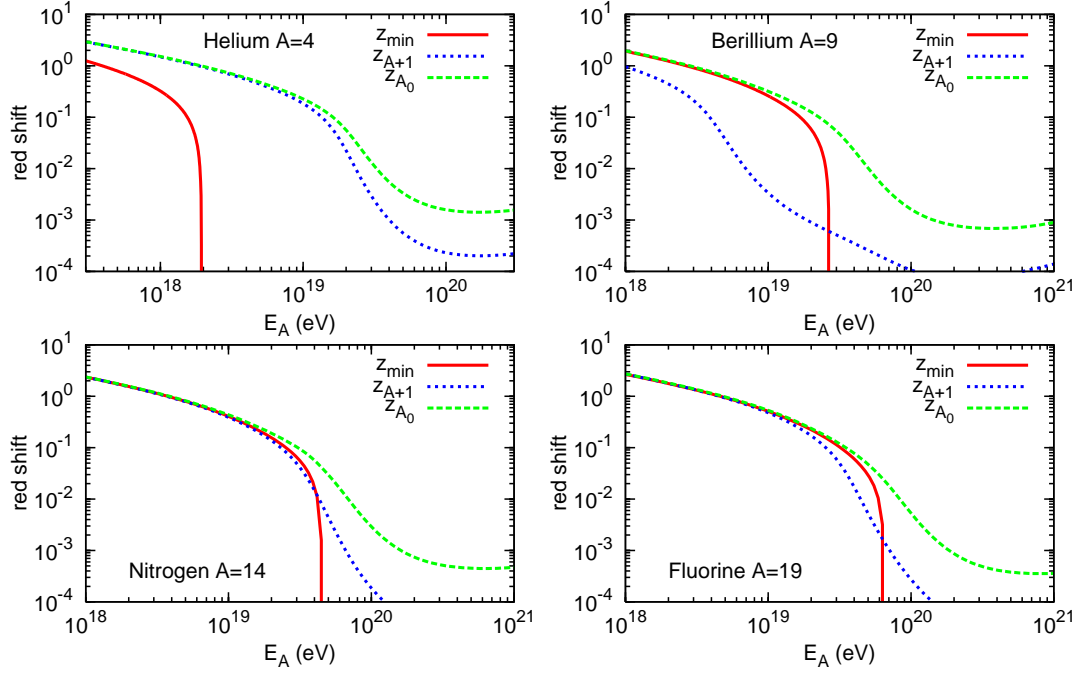


Figure 5: Redshift limits in Eq. (20) for nuclei with small mass number A . The values z_{A+1} and z_{A_0} correspond to redshifts when the running $A(z)$ reaches $A + 1$ and A_0 , respectively.

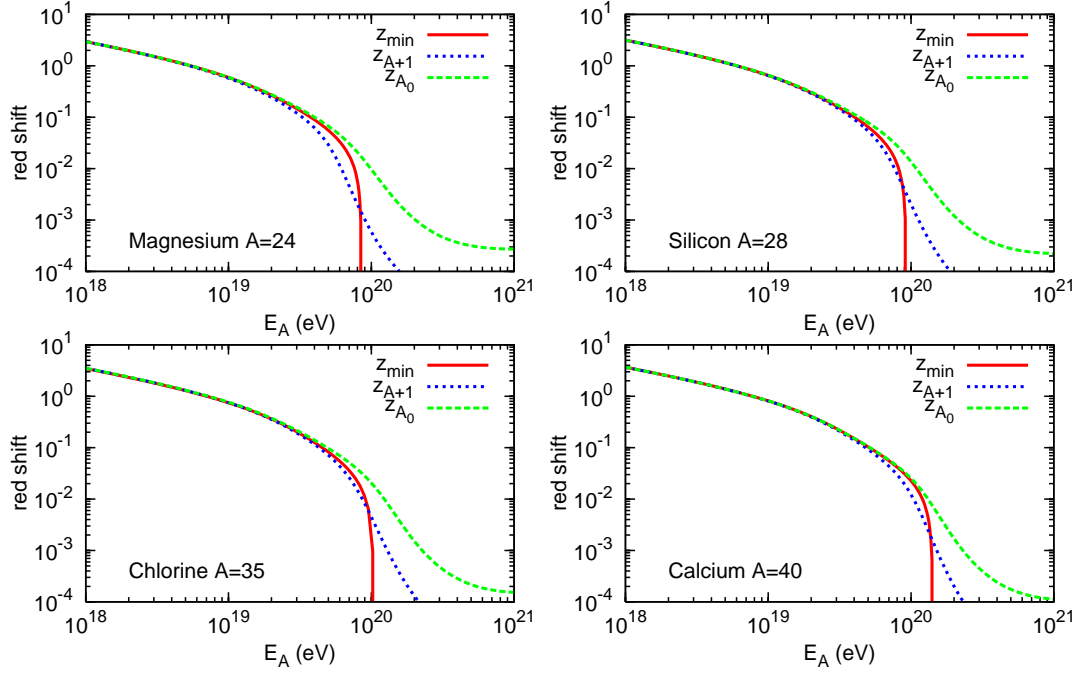


Figure 6: Redshift limits for nuclei with large A . Notation is the same as in Fig. 5.

role of z_{\max} is z_{A+1} , where the running $A(z)$ reaches $A+1$ (solution of $\mathcal{A}(A, \Gamma, z_0 = 0, z) = A + 1$). This value corresponds to $\eta = 1$ and can be calculated from

$$\int_0^{z_{A+1}} dz \left| \frac{dt}{dz} \right| \frac{dA}{dt} = 1. \quad (22)$$

But as a matter of fact a *physical upper limit* appears automatically in Eq. (20) due to the exponential factor $e^{-\eta}$. For any value of z between z_{\min} and z_g in Eq. (20) there is a suppression factor $e^{-\eta(z)}$, which equals to e^{-1} for $z = z_{A+1}$. Even in the case of $z_{\min} > z_{A+1}$ the integral in Eq. (20) is not zero, being however exponentially suppressed. This is a specific feature of the kinetic-equation approach to the problem, and an example when mathematics is more clever than a man.

The calculation of the lower limit of integration in Eq. (20) is more complicated. The lower limit $z_{\min}(\Gamma)$ is provided by vanishing of the generation rate $Q_A(z)$ at $z \leq z_{\min}$. As has been discussed in Section 2.3 at $z=0$ there is a critical Lorentz factor Γ_c^{A+1} below which the photo-disintegration of the parent nucleus $A + 1$ is absent (see Figs. 1 and 2). With increasing z this critical Lorentz factor $\Gamma_c^{A+1}(z)$ slightly diminishes because both the pair production and photo-disintegration curves are shifted in Fig. 2 by factor $(1 + z)$ to lower energies. If Lorentz factor of a considered nucleus $\Gamma < \Gamma_c^{A+1}$, the transition $A \rightarrow (A + 1)$ at $z = 0$ is forbidden and only Γ increases with z (but not A). At z_c when Lorentz factor of A nucleus $\mathcal{G}(A, \Gamma, 0, z_c)$ reaches $\Gamma_c^{A+1}(z_c)$ the photo-disintegration starts (see Eq. 11). Thus, for $\Gamma < \Gamma_c^{A+1}$ $z_{\min}(\Gamma) = z_c(\Gamma)$. For $\Gamma > \Gamma_c$ $z_{\min}(\Gamma) = 0$.

This effect of z_{\min} -appearance can be explained in the evolution-trajectory approach as follows. The production rate of A -nuclei, $Q_A(z)$, is caused by the decay of $A + 1$ nuclei. However, at all z for which $\Gamma_{A+1}(z) < \Gamma_c^{A+1}(z)$ a nucleus $A + 1$ does not decay and $A + 1 = \text{const}$, as we observe indeed in the calculation of the trajectories forward in time, and hence $Q_A(z) = 0$ at $z \leq z_c$.

The lower limit $z_{\min}(\Gamma)$ and the two maximum upper limits z_{A_0} (the largest physically accessible z when the real upper limit is provided by $e^{-\eta}$) and z_{A+1} are shown numerically in Figs. 5 and 6 for low and large A , respectively. One may recognize in these figures the regions in the energy - redshift plane which contribute significantly to the flux of secondary nuclei. In particular, in the case of nuclei with mass number $A \geq 9$ the interval (z_{\min}, z_{\max}) is vanishingly small at low energies, with almost no contribution to the flux, while it becomes non-zero at the highest energies ($E > 10^{19}$ eV). However, at these energies the values of z_{\min} and z_{\max} are constrained to very low values in the range of 10^{-3} , and thus the fluxes are strongly suppressed.

The only exception is represented by secondary Helium. In this case the interval (z_{\min}, z_{\max}) is large and spans over values up to $z = 2$ in a wide energy interval (see upper-left panel of Fig. 5). The peculiar behavior of Helium is connected with its particular production process which is given by the photo-disintegration of Beryllium



Beryllium is photo-disintegrated starting from anomalously low Lorentz factor $\Gamma_c^{\text{Be}} = 5.1 \times 10^8$ (see Fig. 1) lower than that of Helium $\Gamma_c^{\text{He}} = 4.2 \times 10^9$. Born with Γ_c^{Be} , Helium nucleus is practically stable, and thus its flux is large.

3.3 Fluxes of secondary nuclei: calculations

One may notice that the integration in Eq. (20) follows many different evolution trajectories marked by the values $z = z_A$, where transition $A \rightarrow A + 1$ occurs (see left panel of

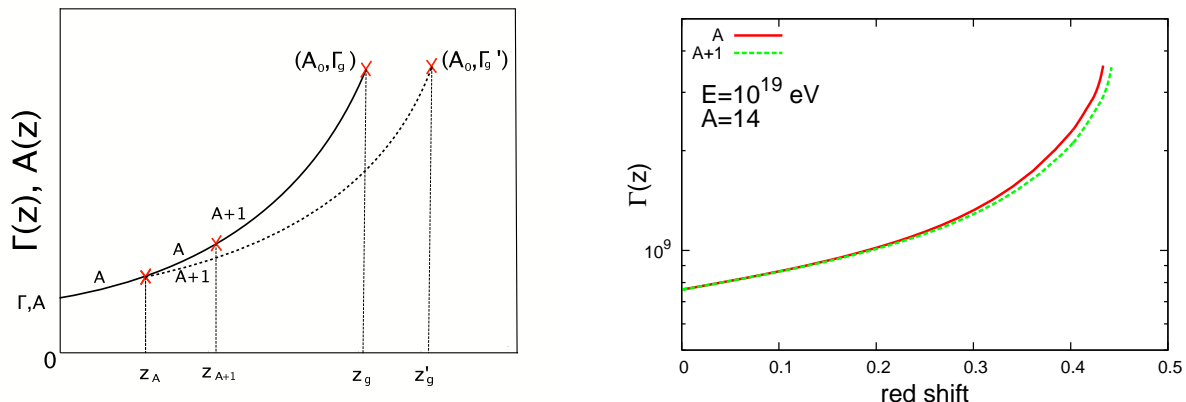


Figure 7: The main (solid curves) and ordinary (dashed curves) trajectories $\mathcal{G}(\Gamma, A, 0, z')$. The left panel shows the sketch, the right panel - the realistic calculations for $A = 14$. In the left panel z_{A+1} is the redshift of $A \rightarrow A + 1$ transition on the main trajectory and z_A , the integral variable in Eq. (20), is the redshift of $A \rightarrow A + 1$ transition on an ordinary trajectory. There are variety of ordinary trajectories starting at different z_A located in the interval (z_A^{\min}, z_{A+1}) .

Fig. 7). We call all of them collectively the *ordinary trajectories*. Among ordinary trajectories we select the particular one, to which we refer as to the *main trajectory*. It corresponds to the transition $A - 1 \rightarrow A$ at $z = 0$, i.e. it follows the evolution $\mathcal{G}(A, \Gamma, z_0 = 0, z)$. In the left panel of Fig. 7 we show as a sketch the main trajectory (solid curve) and one of the ordinary trajectories (dashed curve). Both start from the same Γ at $z = 0$, but from different A' in continuous A-evolution approach. The transitions from A to $A + 1$ are shown by crosses for both trajectories. The main trajectory corresponds to the largest z_A (marked z_{A+1} in Fig. 7) at which transition $A \rightarrow A + 1$ occurs. In principle, A_0 is reached at different sets (z'_g, Γ'_g) for the variety of ordinary trajectories. The right panel displays an example of the real trajectory calculation for $A = 14$ and $E = 1 \times 10^{19}$ eV. The trajectories are very similar indeed and, what is a common feature for all of them, Γ'_g is approximately the same for all of them.

If to use only the main trajectory for calculations, one easily obtains from Eqs. (20), (19), (12) the simple expression:

$$n_A(\Gamma) = \frac{\mathcal{L}_0}{H_0} \frac{\gamma_g - 2}{A_0 m_n} \frac{1}{1 + z_g} \Gamma_g^{-\gamma_g} \frac{d\Gamma_g}{d\Gamma} \int_{z_{\min}(\Gamma)}^{z_g} \frac{dz'}{\sqrt{\Omega_m(1+z')^3 + \Lambda}} e^{-\eta(\Gamma', z')} \quad (23)$$

In Fig. 8 we plot (in arbitrary units) the fluxes of different secondaries (as function of the energy in the left panel and of the Lorentz factor in the right panel) assuming a uniform distribution of sources with Iron as primary ($A_0 = 56$). The injection rate used in Fig. 8 is given by Eq. (12) with a power-law index $\gamma_g = 2.3$. In the left panel we display the comparison of the ordinary-trajectory calculation (solid curves) with the approximate main-trajectory calculation given by Eq. (23) and shown by small filled circles. One can see the precise agreement between both methods, except the case of Helium, where the difference is also small. In the right panel the same spectra are shown as function of the Lorentz factor. In the calculations the maximum energy of acceleration was assumed to be $E_{\max}^{\text{acc}} = Z_0 \times 10^{21}$ eV, as in Eq. (12).

The calculated spectra presented in Fig. 8 correspond to our expectations. The basic parameter which determines the spectra is given by the critical Lorentz factor Γ_c^{A+1} at

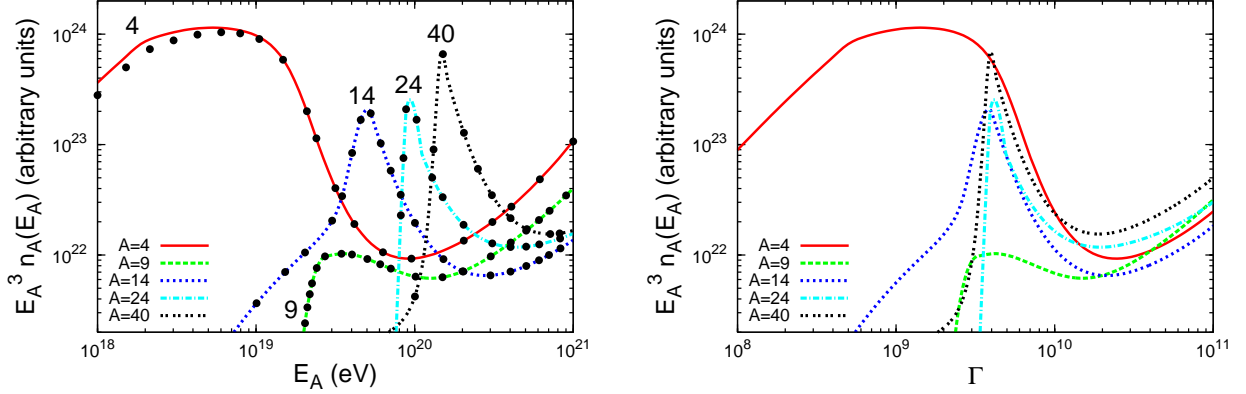


Figure 8: Flux of different secondary nuclei, as function of energy (left panel) and of the Lorentz factor (right panel). The numbers on the curves show A . The small filled circles present fluxes obtained in main-trajectory approximation.

which the photo-disintegration process of the parent nucleus ($A+1$, or Beryllium in the case of Helium) is allowed at $z = 0$. One expects the maximum flux sets at this value of Lorentz factor. As discussed in section 2.1 the critical Lorentz factors are approximately the same for all nuclei, with anomalously low value for ${}^9\text{Be}$. The right panel of Fig. 8 confirms this expectation: all nuclei, but ${}^4\text{He}$ (daughter of ${}^9\text{Be}$), have the maximum at approximately the same $\Gamma \sim \Gamma_c \sim 4 \times 10^9$.

The most spectacular feature of the calculated spectra is the strong dominance of Helium nuclei at low Lorentz factors. As we already discussed above physically it occurs because ${}^4\text{He}$ is born at the decay of ${}^9\text{Be}$ with the same Lorentz factor. But Γ_c for ${}^9\text{Be}$ is the lowest, while for ${}^4\text{He}$ is the highest. Therefore, at low Γ , ${}^4\text{He}$ is stable and its flux is high. From a technical point of view the high flux of ${}^4\text{He}$ is provided by the low z_{\min} , which is also the result of low Γ_c for ${}^9\text{Be}$. Indeed, the $z_{\min} = z_c$ is to be found from the equation $\Gamma_g^{\text{He}}(\Gamma, z_c) = \Gamma_c^{\text{Be}}(z_c)$, which gives low z_c because of the smallness of Γ_c^{Be} . In this respect Helium is much different from all other secondary nuclei. In the case of Helium the redshift region that contributes to the flux is very wide, it spans from $z \sim 10^{-2}$ up to $z \approx 2$ with a large part of the universe contributing to the flux. For secondaries heavier than Helium the contributing universe is vanishingly small, with the relevant redshifts of the order of 10^{-3} or less as follows from curves $z_{A+1}(E)$ in Figs. 5 and 6. Therefore, the fluxes in Fig. 8 for $A \geq 9$ are non-vanishing only because in the present paper we consider an ideal homogeneous distribution of sources with constant density at any redshift, while in a realistic situation the presence of UHECR sources at these low redshifts ($z < 10^{-3}$) is unlikely.

The energy spectrum at high energies follows the corresponding energy losses, with a recovery at the highest energy due to an increase of the nucleus lifetime τ_A (i.e. a decrease in the photo-disintegration energy losses, see Figs. 1 and 2).

The highest energy part of the calculated spectra can be checked with the help of an asymptotic formula obtained from Eq. (23). In the case of very large Γ the term $e^{-\eta}$ may be assumed to be absorbed by $z_{\max} \approx z_{A+1}$, and using $z_{A+1} \ll 1$ and $\Omega_m + \Lambda \approx 1$ one obtains

$$n_A(\Gamma) = \frac{\mathcal{L}_0}{H_0} \frac{\gamma_g - 2}{A_0 m_n} \frac{1}{1 + z_g} \Gamma^{-\gamma_g} \frac{d\Gamma_g}{d\Gamma} z_{A+1}(\Gamma). \quad (24)$$

Eq. (24) describes well the asymptotic regimes in Fig. 8. The smallness of z_{A+1} makes the presence of astrophysical sources at these redshifts rather unrealistic, and the fluxes tends to zero.

As the right panel of Fig. 8 shows, the fluxes of all secondary nuclei at the highest Lorentz factors (corresponding to energies $E \gtrsim 3 \times 10^{19}$ eV) are very low. The physical reason of that is given by the fast destruction of secondary nuclei, so that only small redshifts are accessible as upper limits of integration. At lower Lorentz factors (energies) the redshift range Δz from which a nucleus can be produced and arrive undestroyed is very small. In our calculations it is provided by z_{\min} being very close to z_{\max} (see Figs. 5 and 6). As discussed above the only exception is given by Helium.

4 Secondary nucleons

In this subsection we discuss the flux of secondary nucleons produced in the photo-disintegration of nuclei. We do not need to distinguish neutrons and protons, because at the characteristic lengths involved here neutrons decay fast at all energies of interest. For this reason we will often refer to protons, instead of nucleons.

In contrast to secondary nuclei one expects the larger flux of secondary protons. Indeed, unlike nuclei, protons are not destroyed and can arrive from any redshift, being suppressed only by high energy of generation.

Following the same approach as for secondary nuclei one can write a kinetic equation that describes the propagation of protons:

$$\frac{\partial n_p(\Gamma_p, t)}{\partial t} - \frac{\partial}{\partial \Gamma_p} [b_p(\Gamma_p, t)n_p(\Gamma_p, t)] = Q_p(\Gamma_p, t) \quad (25)$$

where n_p is the secondary-proton density, $b_p = d\Gamma/dt$ describes the loss of proton Lorentz factor (energy loss) due to adiabatic energy losses, pair-production and photo-pion production on the CMB radiation, and Q_p is the generation rate for secondary protons, produced by photo-disintegration of secondary or primary nuclei. The solution of Eq. (25) for protons produced by decay of secondary nuclei with fixed A reads [47]:

$$n_p^A(\Gamma_p) = \int_{z_A^{\min}}^{z_A^{\max}} dz_A \left| \frac{dt_A}{dz_A} \right| Q_p^A(\Gamma_A, z_A) \frac{d\Gamma_A}{d\Gamma_p} \quad (26)$$

Here we use the Lorentz factor equality (13) $\Gamma_g^p \approx \Gamma_A$, where Γ_A is the Lorentz-factor of decaying nucleus A and Γ_g^p is the Lorentz factor of generated proton p . The rate of proton generation at the decay of A is given by the decay rate of nuclei A and as in Eq. (19) we have from conservation of number of particles:

$$Q_p^A(\Gamma_A, z_A) = Q_{A_0}(\Gamma_g, z_g) \frac{1 + z_A}{1 + z_g} \frac{d\Gamma_g}{d\Gamma_A}, \quad (27)$$

where z_A is the redshift of A decay, and Q_{A_0} is the rate of generation (acceleration) of primaries A_0 at redshift z_g with Lorentz factor Γ_g , given by Eq. (12). The generation redshift z_g is determined from $\mathcal{A}(A, \Gamma_A, z_A, z_g) = A_0$ and the generation Lorentz factor is calculated as $\Gamma_g = \mathcal{G}(A, \Gamma_A, z_A, z_g)$. Finally we obtain for n_p^A at $z = 0$:

$$n_p^A(\Gamma_p) = \frac{\gamma_g - 2}{A_0 m_N} \mathcal{L}_0 \int_{z_A^{\min}}^{z_A^{\max}} dz_A \left| \frac{dt_A}{dz_A} \right| \Gamma_g^{-\gamma_g} \frac{1 + z_A}{1 + z_g} \frac{d\Gamma_g}{d\Gamma_A} \frac{d\Gamma_A}{d\Gamma_p}, \quad (28)$$

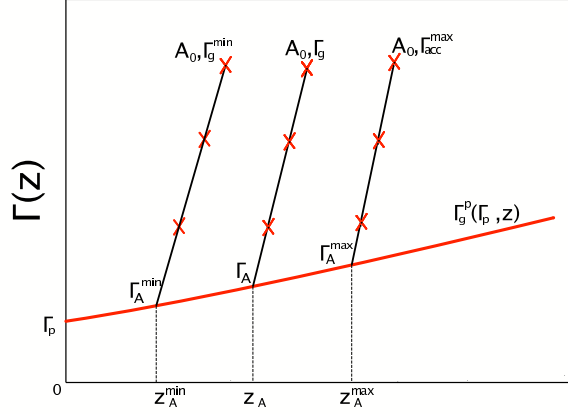


Figure 9: Sketch of evolution trajectories from a proton with Lorentz factor Γ_p at $z = 0$ to a primary nucleus A_0 . The evolution of proton without transition to A-nucleus is shown by the line $\Gamma_g^p(\Gamma_p, z)$. The point of $A \rightarrow (A - 1) + N$ transition is marked by (z_A, Γ_A) . The origin of limiting redshifts z_A^{\min} and z_A^{\max} is explained in the text. The integration in Eq. (28) goes along variety of trajectories $p \rightarrow A_0$, when z_A changes between z_A^{\min} and z_A^{\max} .

where the derivative $d\Gamma_A/d\Gamma_p \equiv d\Gamma_g^p/d\Gamma_p$ (see [2] and [9]) is given by

$$\frac{d\Gamma_A}{d\Gamma_p} = (1+z) \exp \left[\int_0^z dz' \left| \frac{dt}{dz'} \right| (1+z')^3 \left(\frac{db_0^p(\Gamma')}{d\Gamma'} \right)_{\Gamma'=(1+z')\Gamma_A(z')} \right] \quad (29)$$

with $b_0^p(\Gamma) = d\Gamma/dt$ being the energy losses of protons at $z = 0$ and $\Gamma_A(z') = \Gamma_g^p(\Gamma_p, z')$. The derivative $d\Gamma_g^{A_0}/d\Gamma_A$ for nuclei is given in appendix A.

The integration in Eq. (28) goes along variety of trajectories as sketched in Fig. 9. Along these trajectories Γ_g of primary nucleus A_0 and redshifts of generation z_g are different.

The minimum redshift in Eq. (28) is calculated as explained in sections 2.3 and 3.2. If the proton Lorentz factor $\Gamma_p < \Gamma_c^A(0)$ the minimum redshift corresponds to z_c at which the proton Lorentz factor $\Gamma_g^p(z_c)$ reaches the critical Lorentz factor of the A-nucleus $\Gamma_c^A(z_c)$. In the case $\Gamma_p > \Gamma_c$, $z_{\min} = 0$. The maximum upper limit z_{\max} corresponds to the trajectory on which the Lorentz factor of the A_0 -nucleus reaches $\Gamma_{\text{acc}}^{\max}$ (see Fig. 9). These limits are plotted in Fig. 10, with z_{\max} shown by small filled circles. The other upper limit shown by solid red curve is valid for the *instantaneous method* (see below). Here it is important to note that both limits coincide with great accuracy.

The total space density of secondary protons is given by the summation over the primary A_0 and all the secondaries A in Eq. (28):

$$n_p(\Gamma_p) = \sum_{A \leq A_0} n_p^A(\Gamma_p) \quad . \quad (30)$$

Before discussing the numerical results for the calculated flux, we present an alternative and more simple method of calculation, which, being less precise, can be considered as a test for the calculations described above.

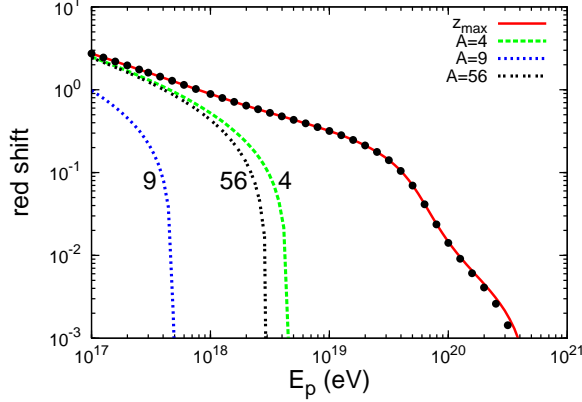


Figure 10: Upper and lower redshift limits in Eq. (28). The lower limits are shown for three nuclei with $A=4$, 9 and 56 and labelled by these numbers. The highest limit for Helium and the lowest for Beryllium are explained by the highest and lowest critical Lorentz factors Γ_c for these nuclei. The lower limits for $A=14, 24, 35$ and 40 (not shown here) are grouped between $A=4$ and 56 . The upper limit (see the text) is given by small filled circles. The full red curve shows the upper limit for the instantaneous approach.

This approach, which will be referred to as “*primary-nucleus instantaneous decay*”, is based on the assumption that at the moment of production z_g the primary nucleus is instantaneously photo-disintegrated to A_0 nucleons. At large Lorentz factors this assumption is well justified because the nucleus lifetime $\tau_{A_0}(\Gamma_g)$ is much shorter than all other relevant time scales of the problem. It is not clear how well this assumption works at lower Lorentz factors and we will show it in our calculations. To distinguish the previous more precise approach from the instantaneous one, we will refer to it as *intermediate A-decay* method.

The proton space density in the instantaneous approach can be written as

$$n_p^{\text{inst}}(\Gamma_p) = A_0 \int_{z_g^{\text{min}}(A_0)}^{z_g^{\text{max}}} dz_g \left| \frac{dt_g}{dz_g} \right| Q_{A_0}(\Gamma_g^p, z_g) \frac{d\Gamma_g^p}{d\Gamma_p}, \quad (31)$$

where all notations are as before, $d\Gamma_g^p/d\Gamma_p$ is given by Eq. (29) and Q_{A_0} by Eq. (12).

Since $Q_{A_0} \propto 1/A_0$, the factor A_0 disappears from Eq. (31) and $n_p^{\text{inst}}(\Gamma_p)$ can depend on A_0 only through the limits of integration.

After a simple rearrangement of Eq. (31) one obtains

$$n_p^{\text{inst}}(\Gamma_p) = \frac{\mathcal{L}_0 \gamma_g - 2}{H_0 m_N} \int_{z_g^{\text{min}}}^{z_g^{\text{max}}} dz_g \frac{[\Gamma_g^p(\Gamma_p, z_g)]^{-\gamma_g}}{(1+z_g)\sqrt{\Omega_m(1+z_g)^3 + \Omega_\Lambda}} \frac{d\Gamma_g^p}{d\Gamma_p}. \quad (32)$$

Eq. (32) is very simple for calculations, because it involves only the *proton trajectory* in $\Gamma - z$ plane (trajectories from A to A_0 in Fig. 9 shrink to a point). The limits of integration are the same as those shown in Fig. 10. The basic observation involved in the calculation of these limits is that the A_0 nucleus is now located on the proton trajectory $\Gamma_g^p(\Gamma_p, z)$ in Fig. 9. Therefore, z_g^{min} is defined by the equation $\Gamma_g^p(\Gamma_p, z_{\text{min}}) = \Gamma_c^{A_0}(z_{\text{min}})$, which is the same as for nuclei A , considered now as A_0 in Fig. 10. The upper limit is defined by the condition $\Gamma_g^p(\Gamma_p, z_{\text{max}}) = \Gamma_{\text{acc}}^{\text{max}}$ and it is shown in Fig. 10 by full red curve,

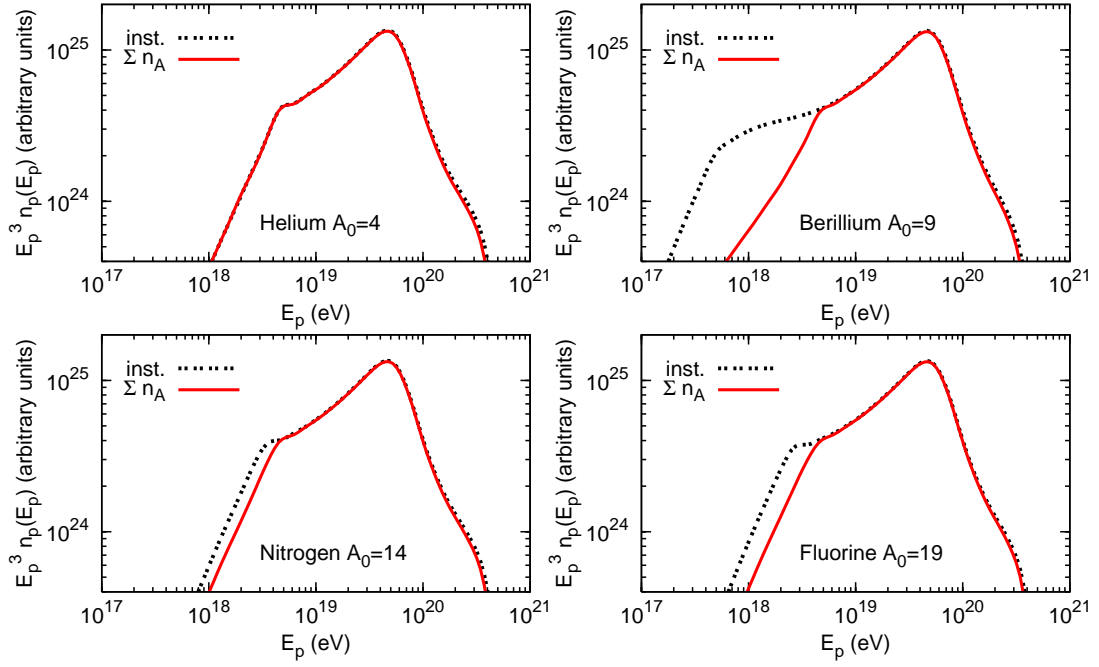


Figure 11: Spectra of secondary-proton computed by the intermediate A-decay method (continuous red curves) and in the instantaneous approximation (black dotted curves) for different A_0 . The generation spectral index is $\gamma_g = 2.3$ in all cases.

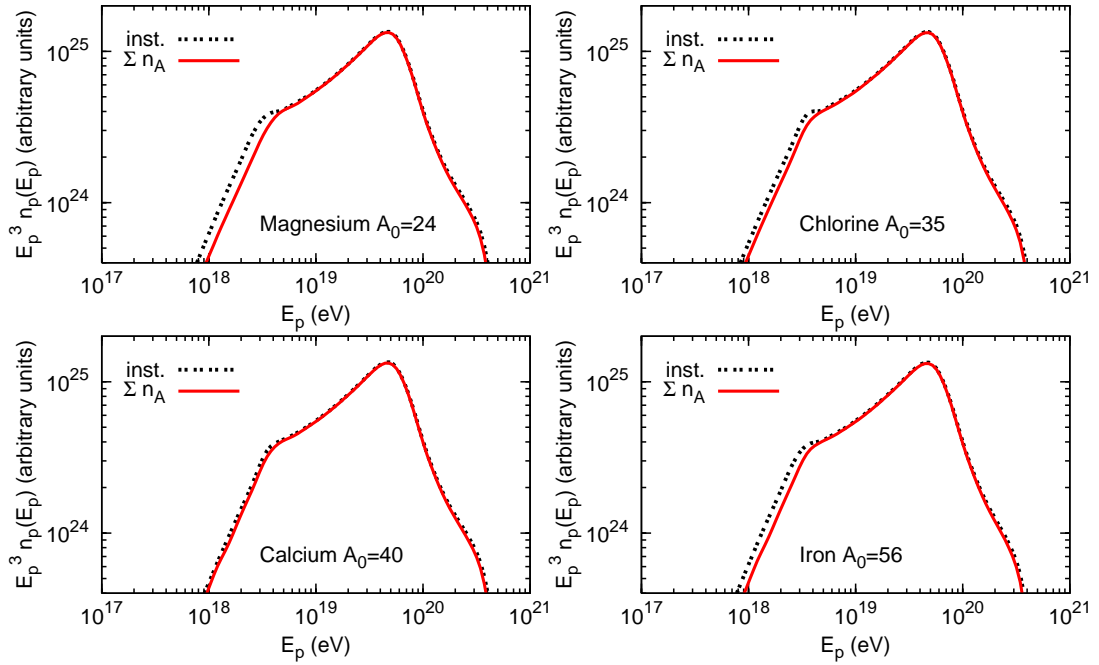


Figure 12: The same as in Fig. 11 for heavy nuclei.

which coincides with upper limit in intermediate A method. We see, thus, that the upper limit z_{\max} does not depend on A_0 . The lower limit at $\Gamma_p \geq \Gamma_c^{A_0}$ is $z_{\min} = 0$. At $\Gamma_p \leq \Gamma_c$ the lower limit depends on A_0 , but weakly, with the exceptional case of Beryllium.

Thus, at high energy when $z_{\min} = 0$ the flux has a universal form independent of the primary nucleus, i.e. of A_0 . It is natural to expect that the high energy regime starts from $\Gamma_p > \Gamma_c^{A_0}$ when $z_{\min} = 0$, and the calculations below confirm this expectation. The high-energy regime is of particular interest as a test of the *intermediate A-decay* method. In this case the proton flux in *instantaneous approximation* n_p^{inst} must coincide with the intermediate A method, when the flux is given by $\sum n_p^A$, i.e. by Eq. (30). Figs. 11 and 12 reliably confirm it, demonstrating that intermediate A method has passed this test.

The case of ${}^4\text{He}$ as primary is very exceptional: the energy threshold of photo-disintegration for ${}^4\text{He}$ is much higher than for its daughter nuclei: ${}^3\text{He}$ and D. Hence, when ${}^4\text{He}$ starts to photo-disintegrate, its daughter-nuclei disintegrate too. Based on this argument we expect that in the Helium case the spectra of secondary protons calculated by both methods should be identical at all Lorentz factors, including the low ones, and this expectation is clearly confirmed by the upper-left panel of Fig. 11. As discussed in section (2.3), in our computation scheme we select allowed trajectories by checking the condition of $A \rightarrow A + 1$ transition, taken in the form $\Gamma_A(z_{A+1}) \geq \Gamma_c^{A+1}(z_{A+1})$. This check is performed along the whole trajectory that goes from A to A_0 (see Fig. 9). In this way we detect the cases when some grand-father or grand-grand-father nucleus has an anomalously high Γ_c and blocks the whole chain. The trajectory opens after increasing z_A^{\min} . In the case of ${}^4\text{He}$ we have also performed the analytic calculations which prove that the proton spectra in the instantaneous and intermediate decays are the same.

We now come over to the "Beryllium excess" in the spectrum of the instantaneous decay, shown in the upper-right panel of Fig. 11. The nature of this effect is simple: $\Gamma_c^{\text{Be}} \ll \Gamma_c^{\text{He}}$ and since ${}^4\text{He}$ is born with Lorentz factor of ${}^9\text{Be}$, the former can be stable and secondary protons are not produced. For $\Gamma > \Gamma_c^{\text{Be}}$ it gives a suppression of the secondary proton flux. Under the assumption of an instantaneous decay this effect is absent.

Beryllium effect works for all $A_0 > 9$ and since it affects only 8 protons from two ${}^4\text{He}$ nuclei, its influence on heavy nuclei is weaker, as one observes from Fig. 12.

The shape of the proton spectra in Figs.11 and 12 can be naturally explained. They have two spectral breaks: the high energy steepening, which is the usual GZK cutoff at energy $E \sim 5 \times 10^{19}$ eV, and the low-energy steepening which coincides with Γ_c ($\sim 5 \times 10^9$ for ${}^4\text{He}$, $\sim 5 \times 10^8$ for ${}^9\text{Be}$ etc). Below Γ_c the adiabatic energy losses dominate and it explains the flat spectrum $n_p(E_p)$ there. It is different from $\propto E^{-\gamma_g}$ because z_{\min} in Eq. (28) and Eq. (32) depends on Γ , i.e. on E_p .

We finish this section with a remark about the universality of the secondary-proton spectrum. Using Eq. (32) for the instantaneous spectrum we proved its universality, i.e. independence of A_0 . The intermediate A spectrum has the same property, since it coincides with the instantaneous one. By other words the normalised spectrum calculated for one A_0 is valid for any other A_0 with the same normalization.

5 Primary nuclei

We calculate here the diffuse flux of primary nuclei A_0 , which arrive undestroyed from the sources. The comoving space density of these nuclei $n_{A_0}(\Gamma, t)$ is described by the kinetic

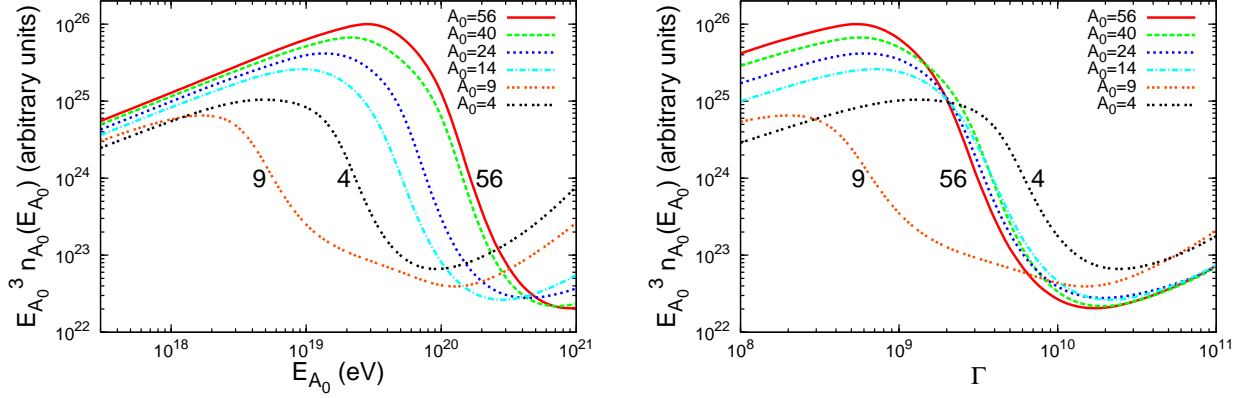


Figure 13: Spectrum of primary nuclei with various A_0 as function of energy (left panel) and Lorentz factor (right panel).

equation

$$\frac{\partial n_{A_0}(\Gamma, t)}{\partial t} - \frac{\partial}{\partial \Gamma} [b_{A_0}(\Gamma, t)n_{A_0}(\Gamma, t)] + \frac{n_{A_0}(\Gamma, t)}{\tau_{A_0}(\Gamma, t)} = Q_{A_0}(\Gamma, t) \quad , \quad (33)$$

where $Q_{A_0}(\Gamma, t)$ is the generation rate of primary nuclei per unit time and comoving volume, and $\tau_{A_0}(\Gamma, t)$ is the photo-disintegration lifetime of the nucleus A_0 calculated as $[A_0\beta_{\text{dis}}(A_0, \Gamma, z)]^{-1}$ with β_{dis} given by Eq. (7).

As found in appendix B the solution of the kinetic equation (33) reads

$$n_{A_0}(\Gamma) = \int_0^\infty dz_g \left| \frac{dt_g}{dz_g} \right| Q_{A_0}(\Gamma_g, z_g) \frac{d\Gamma_g}{d\Gamma} e^{-\eta(\Gamma_g, z_g)} \quad (34)$$

where $n_{A_0}(\Gamma)$ is the space density of nuclei A_0 at $z = 0$, $\Gamma_g = \mathcal{G}(A_0, \Gamma, z_0 = 0, z_g)$ is the Lorentz factor of nuclei A_0 at the moment of generation z_g calculated by the evolution trajectory, with *fixed* A_0 , from Γ at $z_0 = 0$. The ratio $d\Gamma_g/d\Gamma$ is also calculated with fixed A_0 . The quantity η takes into account the photo-disintegration of the propagating nucleus:

$$\eta(\Gamma_g, z_g) = \int_{t(z_g)}^{t_0} \frac{dt}{\tau_{A_0}(\Gamma(t), t)} \quad . \quad (35)$$

The lower limit of integration in Eq. (34) reflects the assumption of an homogeneous distribution of the sources. The upper limit is imposed by the factor $\exp(-\eta)$ accompanied by the condition of a maximum acceleration Lorentz factor: $Q_{A_0}(\Gamma_g) = 0$, if $\Gamma_g \geq \Gamma_{\text{max}}^{\text{acc}}$.

In Fig. 13 we plot the flux of primary nuclei for various A_0 , using the injection spectrum with $\gamma_g = 2.3$. The steepening of the spectra in Fig. 13 starts from the Lorentz factor where pair-production energy losses are equal to adiabatic energy losses. Comparison of Figs. 2 and 13 confirms it. It is worth noting that this criterion for the beginning of the steepening was obtained first in [26].

6 Discussion and Conclusions

We summarize first our approach to the analytic solution of the problem.

We calculate the diffuse spectra of primary and secondary nuclei, and secondary protons for homogeneously distributed sources. With the help of two coupled differential

equations for the propagation of a primary nucleus in the backward time (increasing of the redshift) we find the evolution trajectories $A(z) = \mathcal{A}(A, \Gamma, z_0, z)$ and $\Gamma(z) = \mathcal{G}(A, \Gamma, z_0, z)$, where the first three arguments give the initial conditions. Atomic number A changes continuously, but we interpret this trajectory like in Fig. 3, namely assuming that decays $A + 1 \rightarrow A$ and $A \rightarrow (A - 1)$ occurs instantaneously and a nucleus between these two decays has a fixed atomic number A . Thus, calculated as a continuous quantity $A(z)$ has only an auxiliary meaning. In fact, the trajectories are basically needed to compute Γ_g and z_g , the Lorentz factor of the primary nucleus A_0 at the redshift of its acceleration z_g . We calculate the space density of each species $a = A, p, A_0$ using a kinetic equation

$$\frac{\partial n_a(\Gamma_a, t)}{\partial t} - \frac{\partial}{\partial \Gamma_a} [b_a(\Gamma_a, t)n_a(\Gamma_a, t)] + \frac{n_a(\Gamma_a, t)}{\tau_a(\Gamma_a, t)} = Q_a(\Gamma_a, t), \quad (36)$$

where $b_a = (\beta_{\text{pair}}^a + \beta_{\text{ad}}^a)\Gamma_a$ is the rate of the Lorentz factor loss, $\tau_a(\Gamma_a, z)$ is the photo-disintegration lifetime of particle a (for $a = p$, $\tau_a = \infty$) and $Q_a(\Gamma_a, z)$ is the generation rate of particles a .

For secondary nuclei A and protons produced in the photo-disintegration processes the generation rate $Q_a(\Gamma_a, z)$ is found from the conservation of the number of particles along a trajectory, $dN_a = dN_g$, where dN_g is the number of generated primaries A_0 at acceleration. The relation between the generation rate of primaries A_0 and of secondary A and p is given by Eq. (19), where z_g and Γ_g are calculated using the evolution trajectories. The solutions of the kinetic equations (36) are found analytically.

An important physical quantity in our calculation is the critical Lorentz factor Γ_c^A at epoch $z = 0$. It is determined by the equality in the rates for changing of Γ and A : $\beta_{\text{dis}}^A(\Gamma_c^A) = \beta_{\text{ad}} + \beta_{\text{pair}}^A(\Gamma_c^A)$, where indices 'dis', 'ad' and 'pair' are related to photo-disintegration, adiabatic and pair-production energy losses, respectively. This relation provides a stability condition for the A nucleus at $z = 0$: $\Gamma < \Gamma_c^A$. The critical Lorentz factor Γ_c is a basic energy scale, which gives a key for understanding of all processes considered here and also explains some features seen in the calculated spectra. The condition of allowed trajectories is also given in terms of the critical Lorentz factor $\Gamma_c^A(z)$ determined for epoch z (see Eq. 11).

We will list now the noticeable physical results obtained in this paper.

The fluxes of secondary nuclei have a maximum, which sets at the critical Lorentz factor $\Gamma_c \approx 4 \times 10^{19}$ eV, universal for all heavy nuclei (see Fig. 8). All fluxes are small, except ${}^4\text{He}$ flux, which strongly dominates at $1 \times 10^{18} - 2 \times 10^{19}$ eV. This fact, already known from MC simulations (e.g. see [22]), is well understandable within our approach. ${}^4\text{He}$ nuclei are born from ${}^9\text{Be} \rightarrow 2 {}^4\text{He} + \text{N}$ decay with a characteristic Lorentz factor $\Gamma_c^{\text{Be}} = 5.1 \times 10^8$. Since Γ_c^{He} is much higher (4.8×10^9), the born Helium nuclei are stable (i.e. are not photo-disintegrated) and the flux is high.

The fluxes of secondary protons are higher than that of secondary nuclei, because they are not photo-disintegrated. We calculated the fluxes of secondary protons by two methods. In the first method the protons are produced through each intermediate nucleus in the complete photo-disintegration chain of a primary nucleus A_0 . This is a precise method. The second method is simple, but approximate one. We assume that the generated primary A_0 with $\Gamma_g \geq \Gamma_c(z_g)$ is immediately photo-disintegrated into A_0 nucleons. Not surprisingly these two methods give the same results at large Lorentz factors $\Gamma > \Gamma_c$, because at this Lorentz factors photo-disintegration time-scale is shorter than that of any other relevant process. More surprising is the agreement in the calculated spectra at $\Gamma < \Gamma_c$. To large extent this effect is explained by large Γ_c^A in comparison with the

daughter nuclei of A -nucleus. We explain this effect by the example of ${}^4\text{He}$. The critical Lorentz factor of ${}^4\text{He}$ is much higher than Γ_c of the daughter nuclei ${}^3\text{He}$ and D . At the decay of ${}^4\text{He}$ these nuclei are born with the Lorentz factor of ${}^4\text{He}$ and thus decay fast. The situation is similar for ${}^{40}\text{Ca}$. Actually the difference in the spectra at $\Gamma < \Gamma_c$ is caused by a ‘‘Beryllium effect’’ (see Fig. 11 and the explanation in the text).

The fluxes of secondary protons in terms of Γ , and hence of proton energies, are universal, i.e. they are the same for all A_0 , at least at the high energies. This result is readily explained by the cancellation of the A_0 factors in the number of protons A_0 , produced in instantaneous decay of a primary nucleus, and the factor A_0 in the denominator of Eq. (12), which gives the generation function of A_0 nuclei (see section 4 for more details).

Acknowledgements

We thank Pasquale Blasi and Askhat Gazizov for valuable discussions. The work of RA and VB is partially funded by the contract ASI-INAF I/088/06/0 for theoretical studies in High Energy Astrophysics.

A Ratio of energy intervals at epochs of production and observation

In this appendix we derive the ratio between Lorentz-factor intervals $d\Gamma_g/d\Gamma$ for a nucleus $A(z)$ propagating along the evolution trajectory $\Gamma_g(z) = \mathcal{G}(A, \Gamma, z_0, z)$, where the first three indices describe the initial conditions and z is the running redshift. The meaning of the generation index g here is more general than the epoch of $A(z)$ evolution to A_0 , though it includes this case, too. $\Gamma_g(z)$ means here the Lorentz factor that a nucleus has at the running epoch of evolution z or z_g .

We use here the Lorentz-factor loss for a nucleus A due to pair production as $b_{\text{pair}}^A(\Gamma, z) = -d\Gamma/dt$, and express it through $b_0^p(\Gamma) = -d\Gamma/dt$ for proton at $z = 0$. At epoch z we have

$$b_{\text{pair}}^A(\Gamma, z) = \frac{Z^2(z)}{A(z)}(1+z)^2 b_0^p[(1+z)\Gamma], \quad (37)$$

and we introduce $\bar{k} = \langle Z^2/A^2 \rangle$, assuming it be constant along the evolution trajectory, and using $Z^2/A = \bar{k}A(z)$.

The Lorentz factor of nucleus A along the trajectory can be presented in a general form as

$$\Gamma_g(t_1, t_2) = \Gamma + \int_{t_1}^{t_2} dt' \left[\left(\frac{d\Gamma}{dt'} \right)_{\text{ad}} + \left(\frac{d\Gamma}{dt'} \right)_{\text{pair}} \right] \quad (38)$$

Changing the variable t to z and using $dt = -dz/[(1+z)H(z)]$, we obtain

$$\Gamma_g(z_0, z) = \Gamma + \int_{z_0}^z \frac{dz'}{1+z'} \Gamma_g(z') + \bar{k} \int_{z_0}^z dz' \frac{1+z'}{H(z')} A(z') b_0^p[(1+z')\Gamma_g(z')], \quad (39)$$

Differentiating Eq. (39) in respect to Γ and using

$$\frac{db_0^p(\Gamma')}{d\Gamma} = \frac{\partial b_0^p(\Gamma')}{\partial \Gamma'} \frac{d\Gamma'}{d\Gamma}, \quad (40)$$

one finds for the ratio of Lorentz-factor intervals $y(z) \equiv d\Gamma_g(z)/d\Gamma$:

$$y(z) = 1 + \int_{z_0}^z \frac{dz'}{1+z'} y(z') + \bar{k} \int_{z_0}^z dz' \frac{(1+z')^2 A(z')}{H(z')} y(z') \left(\frac{db_0^p(\Gamma')}{d\Gamma'} \right)_{\Gamma'=(1+z')\Gamma_g(z')}. \quad (41)$$

Differentiating Eq. (41) in respect to z we obtain a differential equation for $y(z)$

$$\frac{1}{y(z)} \frac{dy(z)}{dz} = \frac{1}{1+z} + \frac{\bar{k}}{H_0} \frac{(1+z)^2 A(z)}{\sqrt{\Omega_m(1+z)^3 + \Omega_\Lambda}} \left(\frac{db_0^p(E')}{d\Gamma'} \right)_{\Gamma'=(1+z)\Gamma_g(z)}. \quad (42)$$

The solution of Eq. (42) can be easily found as

$$y(z) \equiv \frac{d\Gamma_g(z)}{d\Gamma} = (1+z) \exp \left[\frac{\bar{k}}{H_0} \int_{z_0}^z dz' \frac{(1+z')^2 A(z')}{\sqrt{\Omega_m(1+z')^3 + \Omega_\Lambda}} \left(\frac{db_0^p(\Gamma')}{d\Gamma'} \right)_{\Gamma'=(1+z')\Gamma_g(z')} \right]. \quad (43)$$

Equation (43) gives the ratio $d\Gamma_g/d\Gamma$, where $d\Gamma$ is the Lorentz-factor interval at the initial state z_0 (with most important case $z_0 = 0$), when a nucleus has fixed A and Lorentz factor Γ , and $d\Gamma_g$ is the interval on the evolution trajectory at redshift z when the atomic number is $A(z)$ and the Lorentz factor is $\Gamma_g(z)$.

In the applications we often need $d\Gamma_g/d\Gamma$ ratio for a fixed A . The most important case is the primary nuclei A_0 . The ratio for fixed A follows trivially from Eq. (43) substituting there $\bar{k}A(z')$ by constant value Z^2/A .

B Solution of the kinetic equation

In this appendix we derive the solution of the kinetic equation for secondary nuclei from which the solutions for primary nuclei and secondary protons can be easily obtained.

We consider the secondary nuclei A being produced homogeneously in the space with the rate $Q_A(\Gamma, t)$ and then propagate as a nucleus species with the fixed (unchanged) A until it is photo-disintegrated. The kinetic equation reads

$$\frac{\partial n_A(\Gamma_A, t)}{\partial t} - \frac{\partial}{\partial \Gamma} [b_A(\Gamma, t) n_A(\Gamma, t)] + \frac{n_A(\Gamma, t)}{\tau_A(\Gamma, t)} = Q_A(\Gamma, t), \quad (44)$$

where $b_A(\Gamma, t)$ is the rate of Lorentz factor loss given by

$$b_A(\Gamma, t) = -\frac{d\Gamma}{dt} = \Gamma H(z) + \frac{Z^2}{A} b_{\text{pair}}^p(\Gamma, z), \quad (45)$$

with $H(z)$ and b_{pair}^p being the Hubble parameter at redshift z and pair-production loss for proton, respectively. The time of photo-disintegration is given by $\tau_A^{-1} = A\beta_{\text{dis}}^A$ or by $\tau_A^{-1} = dA/dt$, see Eq. (7).

The characteristic equation for the kinetic equation (44) reads

$$d\Gamma/dt = -b_A(\Gamma, t). \quad (46)$$

With $\Gamma(t)$ taken on the characteristic in Eq. (44), the term $b_A(\Gamma, t) \frac{\partial n_A(\Gamma, t)}{\partial \Gamma}$ disappears and the kinetic equation (44) takes the form

$$\frac{\partial n_A(\Gamma_A, t)}{\partial t} + n_A(\Gamma, t) \left[-\frac{\partial b_{\text{pair}}^A(\Gamma, t)}{\partial \Gamma} - \frac{\partial b_{\text{ad}}(\Gamma, t)}{\partial \Gamma} + \tau_A^{-1}(\Gamma, t) \right] = Q_A(\Gamma_A, t) \quad (47)$$

Using the notation

$$\begin{aligned} P_1(z) &\equiv \frac{\partial b_{\text{ad}}(z)}{\partial \Gamma} = H(z) \\ P_2(z) &\equiv \frac{\partial b_{\text{pair}}^A(\Gamma, z)}{\partial \Gamma} = \frac{Z^2}{A} (1+z)^3 \left(\frac{\partial b_0^p(\Gamma')}{\partial \Gamma'} \right)_{\Gamma'=(1+z)\Gamma}, \end{aligned} \quad (48)$$

and taking into account that with Γ on the characteristic, time t becomes the only variable, one obtains the solution of Eq. (47) as

$$n_A(t) = \int_{t_g}^t dt' Q_A(t') \exp \left[- \int_{t'}^t dt'' \left(-P_1(t'') - P_2(t'') + \tau_A^{-1}(t'') \right) \right]. \quad (49)$$

Changing the integration variable t to z and using

$$dt = - \frac{dz}{(1+z)H(z)} = - \frac{1}{H_0} \frac{dz}{(1+z)\sqrt{\Omega_m(1+z)^3 + \Omega_\Lambda}}, \quad (50)$$

the solution can be written as

$$\begin{aligned} n_A(\Gamma, z=0) &= \int_0^{z_{\text{max}}} dz' \frac{Q_A[\Gamma'(\Gamma, z')]}{(1+z')H(z')} \times \\ &\exp \left[\int_0^{z'} dz'' \frac{P_1(z'')}{(1+z'')H(z'')} \right] \exp \left[\int_0^{z'} dz'' \frac{P_2(z'')}{(1+z'')H(z'')} \right] \exp \left[- \int_{t'}^{t_0} \frac{dt''}{\tau_A(\Gamma, t'')} \right] \end{aligned} \quad (51)$$

We keep the last integration over t'' to make clear the physical meaning of this integral as a suppression factor for the survival time of nucleus A . The upper limit t_0 is the age of the Universe.

Putting $P_1(z'')$ and $P_2(z'')$ from Eq. (48) into Eq. (51), we find that the product of the first two exponents gives the ratio of energy intervals calculated in appendix A:

$$(1+z') \exp \left[\frac{Z^2}{A} \frac{1}{H_0} \int_0^{z'} dz'' \frac{(1+z'')^2}{\sqrt{\Omega_m(1+z'')^3 + \Omega_\Lambda}} \left(\frac{\partial b_0^p(\Gamma'')}{\partial \Gamma''} \right)_{\Gamma''=(1+z'')\Gamma_g(z'')} \right] = \frac{d\Gamma_g^A(z')}{d\Gamma^A}. \quad (52)$$

Finally, we have

$$n_A(\Gamma, z=0) = \int_0^{z_{\text{max}}} dz' \frac{Q_A[\Gamma'(\Gamma, z')]}{(1+z')H(z')} \frac{d\Gamma'}{d\Gamma} e^{-\eta(\Gamma', z')}, \quad (53)$$

where

$$\eta(\Gamma', z') = \int_{t'}^{t_0} \frac{dt''}{\tau_A(\Gamma'', t'')} = \int_0^{z'} dz'' \frac{1}{(1+z'')H(z'')} \frac{1}{\tau_A(\Gamma'', z'')}. \quad (54)$$

In fact, in Eq. (53) one can put $z_{\text{max}} \rightarrow \infty$ as upper limit, since it is regulated by the factor $\exp[-\eta(\Gamma', z')]$.

The equations (53) and (54) are valid for primary nuclei (A_0, Z_0) and secondary protons; in the latter case one should put $\tau_A \rightarrow \infty$ and $\eta \rightarrow 0$.

References

- [1] K. Greisen, Phys. Rev. Lett. **16** 748 (1966). G.T. Zatsepin and V.A. Kuzmin, Pisma Zh. Experm. Theor. Phys. **4** 114 (1966).

- [2] V. Berezhinsky and S. Grigorieva, *A & A* **199**, 1 (1988).
- [3] V. Berezhinsky, A. Gazizov, M. Kachelriess, *Phys. Rev. Lett.* **97**, 231101 (2006).
- [4] R. U. Abbasi [HiRes collaboration], astro-ph/0707.2638
- [5] T. Yamamoto et al. [Pierre Auger Collaboration], astro-ph/0703099.
- [6] A. A. Watson, Highlight talk at ICRC 07, arXiv:0801.4050.
- [7] K-H Kampert, arXiv:0801.1986.
- [8] V. Berezhinsky, A. Gazizov and S. Grigorieva, *Phys. Lett.* **B612** 147 (2005).
- [9] V. Berezhinsky, A. Gazizov and S. Grigorieva, *Phys. Rev.* **D74** 043005 (2006). hep-ph/0204357v1.
- [10] R. Aloisio, V. Berezhinsky, P. Blasi, A. Gazizov, S. Grigorieva and B. Hnatyk, *Astrop. Phys.* **27** 76 (2007).
- [11] V. Berezhinsky, A. Gazizov, S. Grigorieva, arXiv:astro-ph/0702488 .
- [12] T. Abu-Zayyad et al [HiRes collaboration] 2002a, astro-ph/0208243;
T. Abu-Zayyad et al [HiRes collaboration] 2002b, astro-ph/0208301.
- [13] T. Abu-Zayyad et al, *Astrophys. J.* **557**, 686 (2001);
T. Abu-Zayyad et al, *Phys. Rev. Lett.*, **84**, 4276 (2000).
- [14] A. V. Glushkov et al [Yakutsk collaboration], *JETP Lett.* **71**, 97 (2000);
A. V. Glushkov and M. I. Pravdin, *JETP Lett.* **73**, 115 (2001).
- [15] D. Bird et al, *Phys. Rev. Lett.*, **71**, 4276 (1993)
D. J. Bird et al [Fly's Eye collaboration], *Ap. J.*, **424**, 491 (1994)
D. J. Bird et al, *Ap.J.* **441**, 144 (1995).
- [16] M. Ave et al, *Astroparticle Phys.*, **19**, 61 (2003).
- [17] K. Shinozaki et al, *Proc. of 28th International Cosmic Ray Conference (ICRC)*, **1**, 401 (2003).
- [18] M. Unger et al. (Pierre Auger Collaboration), astro-ph/0706.1495 .
- [19] M. Nagano and A. Watson, *Rev. Mod. Phys.* **72**, 689 (2000).
- [20] A. Watson, *Nucl. Phys. B (Proc. Suppl.)* **136**, 290 (2004).
- [21] R. Aloisio, V. Berezhinsky, P. Blasi, S. Ostapchenko, *Phys. Rev.* **D77** (2008) 025007.
- [22] D. Allard, E. Parizot, E. Khan, S. Goriely and A.V. Olinto, *A & A* **443** (2005) L29.
D. Allard, A.V. Olinto and E. Parizot, astro-ph/0703633.
- [23] J. Abraham et al. (Pierre Auger Collaboration), *Science* **318** 938 (2007).
- [24] F. W. Stecker, *Phys. Rev.* **180**, 1264 (1969).
- [25] J. L. Paget and F. W. Stecker, *Proc. of 14th ICRC 1975 Munich*, **2** 734 (1975).
- [26] V.S. Berezhinsky, S. I. Grigorieva, G.T. Zatsepin, *Proc. of 14th ICRC (Munich 1975)* **2**, 711 (1975).
- [27] A. M. Hillas, *Proc. of 14th ICRC (Munich 1975)* **2**, 717 (1975).
- [28] J.L. Puget, F.W. Stecker and J.H. Bredekamp, *Astrophys. J.* **205** (1976) 638.
- [29] F.W. Stecker and M.H. Salamon, *Astrophys. J.* **512** (1999) 521.

- [30] E. Khan, S. Goriely, D. Allard, E. Parizot, T. Suomijarvi, A.J. Koning, S. Hilaire and M.C. Duijvestijn *Astropart. Phys.* **23** 191 (2005).
- [31] K. Arisaka, G.B. Gelmini, M. Healy, O. Kalashev and J. Lee, *JCAP* **0712** 002 (2007).
- [32] D. Hooper, S. Sarkar, A. M. Taylor, arXiv:0802.1538.
- [33] L. A. Anchordoqui, M. T. Dova, L. N. Epele and J. D. Swain, *Phys. Rev.* **D57** (1998) 7103.
- [34] L.N. Epele and E. Roulet, *JHEP* **9810** 9 (1998).
- [35] G. Bertone, C. Isola, M. Lemoine and G. Sigl, *Phys. Rev.* **D66** (2002) 103003.
- [36] T. Yamamoto, K. Mase, M. Takeda, N. Sakaki and M. Teshima, *Astrop. Phys.* **20** 405 (2004).
- [37] D. Hooper, A. Taylor and S. Sarkar, *Astropart. Phys.* **23** (2005) 11.
- [38] M. Ave, N. Busca, A. V. Olinto, A. A. Watson and T. Yamamoto, *Astropart. Phys.* **23** (2005) 19.
- [39] E. Armengaud, G. Sigl and F. Miniati, *Phys. Rev.* **D72** (2005) 043009.
- [40] G. Sigl and E. Armengaud, *JCAP* **0510** (2005) 016.
- [41] D. Harari, S. Mollerach and E. Roulet, *JCAP* **0611** (2006) 012.
- [42] D. Allard, E. Parizot and A. V. Olinto, *Astropart. Phys.* **27** (2007) 61.
- [43] D. Hooper, S. Sarkar and A. M. Taylor, *Astropart. Phys.* **27**, 199 (2007).
- [44] L. A. Anchordoqui, H. Goldberg, D. Hooper, S. Sarkar and A. M. Taylor, *Phys. Rev.* **D76** (2007) 123008.
- [45] V. Berezhinskii, S. Bulanov, V. Dogiel, V. Ginzburg, V. Ptuskin, *Astrophysics of Cosmic Rays*, North-Holland, 1990.
- [46] D.N. Spergel *et al.* [WMAP Collaboration], *Astrophys. J. Suppl.* **148** (2003) 175.
D.N.Spergel et al., *Ap.J.S.* **170**, 377 (2007).
- [47] R. Aloisio and V. Berezhinsky, *Ap.J.* **612**, 900 (2004).